DEPARTMENT OF MECHANICAL ENGINEERING AND MECHANICS
COLLEGE OF ENGINEERING AND TECHNOLOGY
OLD DOMINION UNIVERSITY
NORFOLK, VIRGINIA 23508

STUDIES ON CHEMOVISCOSITY MODELING FOR THERMOSETTING RESINS

By

J. M. Bai, Graduate Research Assistant

T. H. Hou, Co-Principal Investigator

and

S. N. Tiwari, Principal Investigator

Progress Report
For the period ended January 31, 1987

Prepared for the
National Aeronautics and Space Administration
Langley Research Center
Hampton, Virginia 23665

Under
Research Grant NAG-1-569
Robert M. Baucom, Technical Monitor
MD-Polymeric Materials Branch

May 1987

DEPARTMENT OF MECHANICAL ENGINEERING AND MECHANICS
COLLEGE OF ENGINEERING AND TECHNOLOGY
OLD DOMINION UNIVERSITY
NORFOLK, VIRGINIA 23508

STUDIES ON CHEMOVISCOSITY MODELING FOR THERMOSETTING RESINS

By

J. M. Bai, Graduate Research Assistant

T. H. Hou, Co-Principal Investigator

and

S. N. Tiwari, Principal Investigator

Progress Report
For the period ended January 31, 1987

Prepared for the
National Aeronautics and Space Administration
Langley Research Center
Hampton, Virginia 23665

Under
Research Grant NAG-1-569
Robert M. Baucom, Technical Monitor
MD-Polymeric Materials Branch

Submitted by the
Old Dominion University Research Foundation
P.O. Box 6369
Norfolk, Virginia 23508

May 1987

FOREWORD

This report covers the work completed on the research project "Chemoviscosity Modeling for Thermosetting Resins" for the period ended January 31, 1987. The work was supported by the NASA Langley Research Center (Polymeric Materials Branch of the Materials Division) under research grant NAG-1-569. The grant was monitored by Mr. Robert M. Baucom of the Polymeric Materials Branch.

STUDIES ON CHEMOVISCOSITY MODELING FOR THERMOSETTING RESINS

By

J. M. Bai[1], T. H. Hou[2], and S. N. Tiwari[3]

SUMMARY

A new analytical model for simulating chemoviscosity of thermosetting resins has been formulated. The model is developed by modifying the well-established Williams-Landel-Ferry (WLF) theory in polymer rheology for thermoplastic materials. By introducing a relationship between the glass transition temperature Tg(t) and the degree of cure $\alpha(t)$ of the resin system under cure, the WLF theory can be modified to account for the factor of reaction time. Temperature-dependent functions of the modified WLF theory constants $C_1(t)$ and $C_2(T)$ were determined from the isothermal cure data. Theoretical predictions of the model for the resin under dynamic heating cure cycles were shown to compare favorably with the experimental data. This work represents progress toward establishing a chemoviscosity model which is capable of not only describing viscosity profiles accurately under various cure cycles, but also correlating viscosity data to the changes of physical properties associated with the structural transformation of the thermosetting resin systems during cure.

[1]Graduate Research Assistant, Department of Mechanical Engineering and Mechanics, Old Dominion University, Norfolk, Virginia 23508.
[2]Adjunct Assistant Professor, Department of Mechanical Engineering and Mechanics, Old Dominion University, Norfolk, Virginia 23508.
[3]Eminent Professor, Department of Mechanical Engineering and Mechanics, Old Dominion University, Norfolk, Virginia 23508.

TABLE OF CONTENTS

TABLE OF CONTENTS - Continued

LIST OF TABLES

LIST OF FIGURES

TABLE OF CONTENTS - Continued

LIST OF FIGURES - Continued

TABLE OF CONTENTS - Concluded

LIST OF FIGURES - Concluded

LIST OF SYMBOLS

a	constant used in Eq. (4.4a)
A_1	material parameter
A_2	material parameter
A_3	material parameter
b	constant used in Eq. (4.4a)
B	material parameter
B'	material parameter
B''	material parameter
c	constant used in Eq. (4.4a)
$C_1(T)$	temperature-dependent parameter of WLF
$C_2(T)$	temperature-dependent parameter of WLF
d	constant used in Eq. (4.4a)
d_1	temperature-dependent parameter
d_2	temperature-dependent parameter
DSC	differential scanning calorimeter
ΔE_1	Arrhenius activation energy
ΔE_2	Arrhenius activation energy
ΔE_3	Arrhenius activation energy
ΔE_k	Arrhenius activation energy of chemical reaction
ΔE_η	Arrhenius activation energy of viscous flow
f	fractional free volume at temperature T
fg	fractional free volume at glass transition temperature Tg
H	heat of reaction
H_T	total heat of reaction
ΔH	transition energy associated with a transition of material
k	kinetic factor
k'	heating rate
k_∞	pre-exponential kinetic factor
K	calibration constant of DSC
K_{n_1}	material constant

K_{n_2}	material constant
K_{n_3}	material constant
R	universial gas constant
R_r	setting of TEMP CALIB RANGE control of DSC
ΔR	number of divisions changed required to adjust R_r
S	speed of chart recorder
t	curing time
t_c	curing time define in Eq. (4.15)
t_f	curing time required for completion of cure
Δt	time interval
T	temperature
T_c	curing temperature
Tg	glass transition temperature
ΔT_{ACT}	difference between measured transition temperature of two materials
ΔT_{IND}	difference between actual transition temperature of two materials
V	free volume of material
V_f	free volume at glass transition temperature
W	weight of material sample
ΔW	setting of ΔW BALANCE control
WLF	Williams-Landel-Ferry

Greek Letter

α	degree of cure
α_f	thermal expansion coefficient
β	angle of baselines between two coordination systems
η	viscosity
η_∞	pre-exponential constant
η_{Tg}	viscosity at glass transition temperature

Chapter 1

INTRODUCTION

Perhaps the single most important property of a polymer with regard to specifying its processing characteristics is its viscosity. Viscosity governs the resin flow characteristics. For thermoplastic materials, the viscosity is influenced by local flow geometry and can vary with processing temperature and shear rate. Viscosity control becomes more critical and difficult in the processing of thermosetting resins, because of the onset of chemical reactions and the generation of heat during cure which causes the viscosity to vary with time. The term chemoviscosity refers to the variation of viscosity due to the polymer chemical reaction. The study of chemoviscosity is generally called chemorheology [1]*.

In a typical autoclave operation for the fabrication of composite materials, the viscosity-time profile must allow first for the bubbling off of trapped gas, then fiber compaction with resin flow, and finally, laminate consolidation under applied pressure before the resin has gelled and ceases to flow. A typical cure cycle for the MACNAMITE AS4/3501-6 graphite pregreg (an amine-cured epoxy resin, Hercules 3501-6, reinforced with unidirectional graphite fibers [2]) is shown in Fig. 1.1.

*The numbers in brackets indicate references.

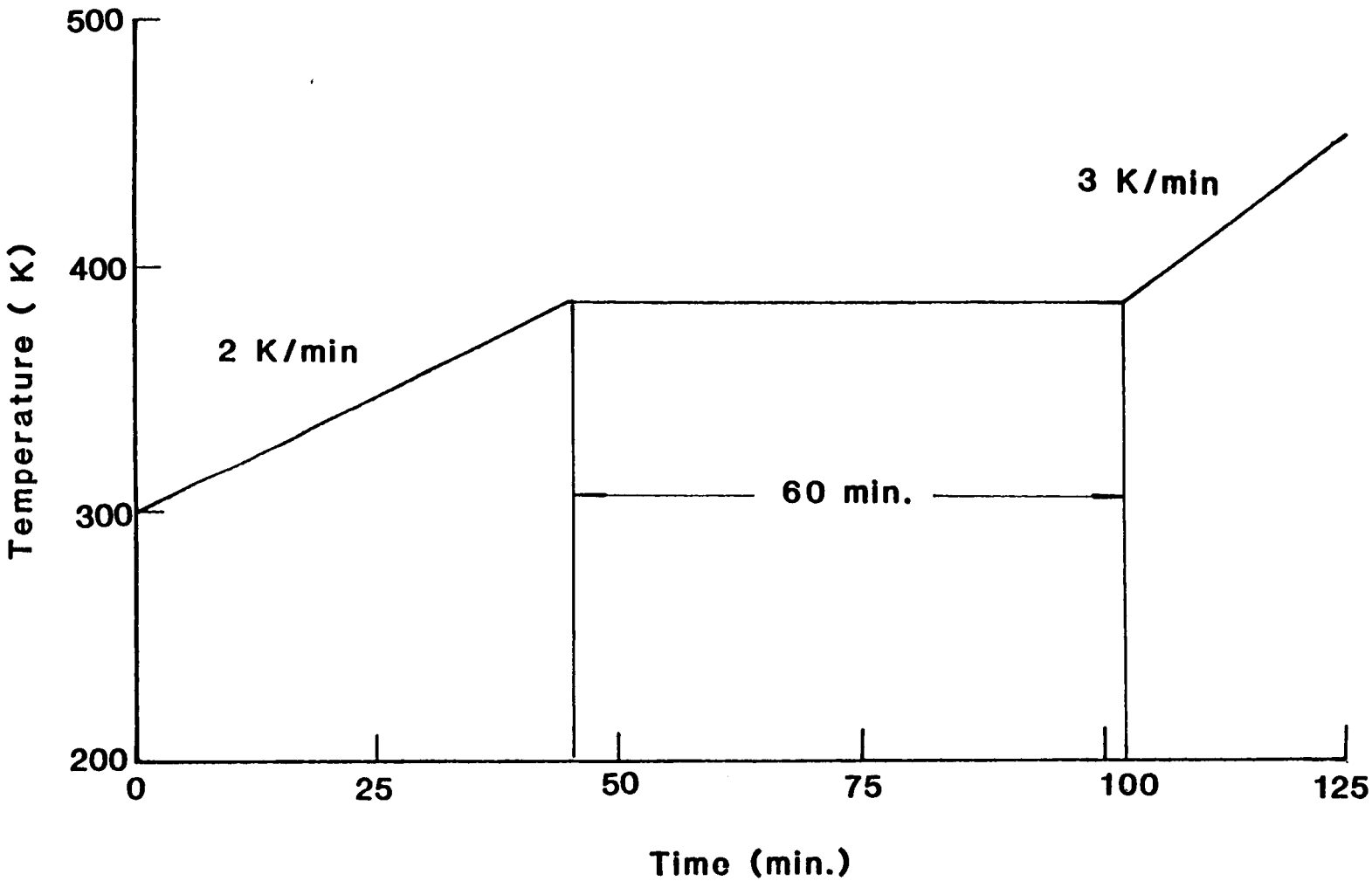

Fig. 1.1 A typical cure cycle for the MACNAMITE AS4/3501-6 graphite pregreg.

At the start of a cure cycle, the polymerization reaction begins and the polymers chains lengthen. The increase in viscosity of the resin due to polymerization is, however, largely offset by the increase in temperature which is introduced through the cure cycle and the heat of reaction. Consequently, a drop in resin viscosity of two or three orders of magnitude at the initial stage of cure is not uncommon. As the resin continues to polymerize, crosslinks are formed and the viscosity of the resin system starts to increase at a faster rate. Finally, the rate of increase of viscosity approaches infinity at gelation. Therefore, any chemoviscosity profile is closely related to the reaction kinetics of the resin systems and the cure cycle (temperature profile) during processing. A fundamental understanding of the chemoviscosity kinetics of thermosetting resin has been necessary in order to obtain a precise processing control.

The objective of present research is to establish a chemoviscosity model which is capable of not only describing viscosity rise profiles accurately under various cure cycles, but also correlating viscosity data to the changes of physical properties associated with the structural transformation of the thermosetting resin systems during cure.

The thermal analysis and rheological analysis on net resin system were conducted by the differential scanning calorimetry and rheometry, respectively, during the course of the study. By introducing a well-established viscosity-temperature relationship already existing in polymer rheology based on the information of thermal analysis and rheological analysis, an analytical model for chemoviscosity profile of thermosetting resin during cure was formulated. The viscosity

calculated by the proposed model could be correlated with the physical properties through the two temperature-dependent functions $C_1(T)$ and $C_2(T)$ as well as the glass transition temperature. In the following chapters, the experimental measurements on the thermal and rehological properties are first introduced and the modeling approaches and results are then presented.

Chapter 2

LITERATURE SURVEY

Numerous researchers have devoted considerable efforts to establish an analytical model for the chemoviscosity growth profile of thermosetting resins under curing. There are two different basic approaches in chemoviscosity modeling of thermosetting resin. The most common approach to the problem has been by empirically specifying the viscosity linearly as an exponential function of reaction [3,4], or with the aid of DSC thermal analysis, the degree of cure [5].

The empirical model proposed by Roller [3] to correlate isothermal viscosity data for a curing B-staged epoxy resin can be expressed as

$$\ln \eta = \ln \eta_0 + kt \tag{2.1}$$

where η is the time dependent viscosity, η_0 is the zero-time viscosity, k is an apparent kinetic factor, and t is the time. Taking the temperature dependence into account, η_0 could be expressed as

$$\eta_0 = \eta_\infty \exp(\Delta E/RT) \tag{2.2}$$

where η_∞ is the pre-exponential constant, ΔE_η is Arrhenius activation energy of viscous flow, and R, the universal gas constant. Similarly, one can also express k with an Arrhenius expression

$$k = k_\infty \exp(-\Delta E_k/RT) \tag{2.3}$$

Here ΔE_k is the Arrhenius activation energy of chemical reaction. Substituting Eqs. (2.2) and (2.3) into Eq. (2.1), we have

$$\ln \eta(t)_T = \ln \eta_\infty + \frac{\Delta E_\eta}{RT} + t\, k_\infty \exp\left(-\frac{\Delta E_k}{RT}\right) \tag{2.4}$$

In the dynamic heating case, cure cycle is a function of time, i.e., $T = T(t)$, and therefore, Eq. (2.4) can be generalized to

$$\ln \eta(t,T) = \ln \eta_\infty + \frac{\Delta E_\eta}{RT} + \int_0^t k_\infty \exp\left(-\frac{\Delta E_k}{RT}\right) dt \tag{2.5}$$

In comparing the calculated viscosity by Eq. (2.5) to the experimental values, Roller [3] noted that there exists a large discrepancy, especially in the higher heating rate cases. It seemed that such empirical simulation of chemoviscosity is inadequate in describing accurately the non-linearity of the chemoviscosity-time profile associated with the advancement of resin under dynamic heating cure cycle. The model is also found to be very much batch-specific and cannot be related directly to the resin chemistry.

In a similar manner, Carpenter [4] adopted the model given in Eq. (2.1) to simulate chemoviscosity of Hercules 3501-6 net resin system, which was cured under various conditions. The kinetics factor k in Eq. (2.1) was expressed as a different function of temperature than that of Roller. When comparing with the experimental values, however, similar inadequancies as those discussed above on Roller's modeling were also noted.

Efforts were also made to model the time-dependence viscosity by Lee et al. [5]. The degree of cure of the reactive resin system during cure was introduced in chemoviscosity modeling by means of DSC. The model for isothermal case has been proposed as follows:

$$\ln \eta = A + k\ \alpha(t) \tag{2.6}$$

where

$$A = \ln \eta_{\infty} + \frac{\Delta E_{\eta}}{RT}$$

ΔE_{η} is the activation energy for viscous flow and k is a constant which is independent of temperature. The viscosity in the dynamic case was obtained from Eq. (2.6). The temperature was calculated from the heating rate at every 0.5 seconds and the values were determined by numerical integration of reaction kinetics which was determined as a priority in the isothermal case. When compared with experimental data, it is seen that Eq. (2.6) is capable of describing the isothermal viscosity well; however, it is inadequate to model the non-linearity of chemoviscosity under the dynamic cure case. This approach, however, has suggested a way of relating chemoviscosity to a physical property, i.e. the degree of cure, which represents the various structure status of a reactive resin system under cure.

The second approach is based on a modification to the well-established viscosity-temperature relationship existing in polymer rheology for thermoplastic materials. The parameters in such an equation can be expressed in terms of polymerization kinetics, and the chemoviscosity profiles as a function of reaction time can then be modeled for thermosetting resin system.

The viscosity-temperature relationship, which is based on the Williams-Landel-Ferry (WLF) theory [6], is given by

$$\text{Log}\left(\frac{\eta_T}{\eta_{Tg}}\right) = \frac{-C_1\ (T-Tg)}{C_2 + T-Tg} \tag{2.7}$$

where C_1 and C_2 are two material constants, and η_{Tg} represents the viscosity at the glass transition temperature Tg of the given thermoplastic material. The normal use of the WLF equation for thermoplastic materials requires that Tg be constant while the temperature T is varied within 100 K above Tg for the specific polymer under study, and Tg can be replaced by any reference temperature Ts within the experimental range. It has been extensively documented in the literature that temperature-dependent viscosity of thermoplastic materials can be accurately described by the WLF equation within 100 K above its glass transition temperature Tg. However, during the curing of thermosetting resins, the monomers are initially polymerized and crosslinks are formed later. This is a system where Tg(t) is changing and the curing temperature T is held constant (in an isothermal cure case, for example). The glass transition temperature Tg rises continuously and may eventually approach the curing temperature. Over the entire curing cycle, the material structure actually undergoes continuous phase transformation from a low molecular weight liquid to a high molecular weight polymeric melt, and eventually transforms to a crosslinked network. For a thermosetting resin system under cure, it is reasonable to assume that Tg(t) of the material is always within 100 K lower than the cure temperature. The WLF equation should then be applicable to every instant state of the resin system under curing. The central theme in modifying the WLF theory to describe the chemoviscosity of thermosetting resin is to take into account the reaction time factor.

The applicability of the modified WLF theory in chemoviscosity modeling for thermosetting resin has been studied by Tajima and Crozier [1,7], Apicella et al. [8] and Hou [9] among others.

Tajima and Crozier [1,7] modeled the chemoviscosity as a function of polymerization kinetics for an amine (DDS)-cured epoxy resin by a modified WLF equation. The advancement of reaction was determined by the concentration of the hardener DDS. The parameters Ts and $\eta(Ts)$ in Eq. (2.7) were allowed to vary with times. The two material parameters C_1 and C_2 were assumed to be independent of reaction time. A fairly good agreement between calculated and experimental data was observed.

In his investigation, Hou [9] proposed an analytical model which was also based on modification of the WLF theory. Major assumptions involved were that the rate of reaction is diffusion controlled and was linearly inversely proportional to the viscosity of the medium over the entire cure cycle. The modified WLF equation became a first order ordinary nonlinear differential equation. Numerical solutions were also shown to compare favorably with the experimental results for several thermosetting systems under isothermal and dynamic heating cure conditions. It was demonstrated [9] that by such modified WLF equation, an analytical model with high degree of accuracy for the chemoviscosity simulation for any thermosetting resin system under various cure cycles can be established. The physical significances of the material parameters selected for the model were, however, difficult to extract for the particular resin system under investigation.

A new approach in chemoviscosity modeling used in the present study will be formulated and discussed later in Chap. 5.

Chapter 3

EXPERIMENTAL METHODS

3.1 Thermal Analysis

3.1.1 Sample Preparation

Sample ranging from 3 to 7 mg in weight was encapsulated in a standard aluminum sample pan. To prevent the sample holder being contaminated by the splitted sample, a small hole was made on the center of the lid. Tweezers were used throughout all the time for sample handling, loading and storing. The weight of the sample was measured before and after the test. The weight losses during the tests were found to be negligible. The prepared samples were stored in a refrigerator and removed just prior to the measurement.

3.1.2 Apparatus

Perkin-Elmer differential scanning calorimeter (Model DSC-2) coupled to a high quality potentionetric recorder (Model 3314, a product of SOLTEC CORP.) was used in thermal analysis.

The DSC is a sophisticated instrument for the measurement and characterization of the thermal properties of materials. It consists of an analyzer desk, draft shield, sample holder cover kit, concealed control panel cover, vacuum pickup device, etc.

When a transition such as melting, boiling and dehydration of crystallization occurs in the sample material, an endothermic or exothermic reaction takes place. The change in power required to maintain the sample holder at the same temperature as the reference temperature (i.e. its programmed temperature) during the transition is recorded as a peak. The chart abscissa indicates the transition temperature and the peak area indicates the total energy transfer to or from the sample. This direct calorimetric measuring principle of the instrument requires that each sample holder has a built-in heater and a temperature sensor.

In the present work, the DSC-2 was upgraded to provide extra cooling capacity which can support operations down to -40°C by means of Intercooler II. In order to prevent moisture condensations on the sample holders while operated in the subambient environment, a package of intermediate range subambient accessory has also been installed. The heating chamber is enclosed in a dry box, and the sample holders can only be accessed through dry box gloves. A nitrogen purge gas line has been connected as well. Dry box is always purged with nitrogen before measurements started. The apparatus was installed in an air-conditioned room maintained at 20°C and 50% relative humidity.

3.1.3 Calibration

The DSC-2 calibrations include the following: temperature (abscissa), energy (ordinate), a conversion constant K determination and the baseline optimization. All calibrations were performed by following the procedure recommended by the manufacturer [10].

Three standard materials, Indium, Zinc and Potassium Chromate were used in the calibration. The characteristics of these three materials are given as follows:

	Transition Point (K)	Transition Energy (cal/gm)
Indium	429.78	6.80
Zinc	692.65	25.90
K2CrO4	943.7±0.5	8.50

The temperature calibration is accomplished with the TEMP CALIB and TEMP CALIB RANGE controls of DSC-2. The construction for determining transition temperature is shown in Fig. 3.1.

By scanning standard materials dynamically at a given rate, transition can be observed and the transition temperature can be determined. The comparison between measured temperature and actual reference temperature can then be made. The following equation was used to determine the change required in the setting of the TEMP CALIB RANGE control.

$$\Delta R = Rr^2 \left[\frac{\Delta T_{IND} - \Delta T_{ACT}}{\Delta T_{ACT}}\right] \left[\frac{1}{1000}\right] \qquad (3.1)$$

where

ΔR ---- number of divisions change required to adjust TEMP CALIB RANGE control

Rr ---- setting of TEMP CALIB RANGE control

ΔT_{IND} ---- difference between measured transition temperatures

ΔT_{ACT} ---- difference between the actual reference temperatures

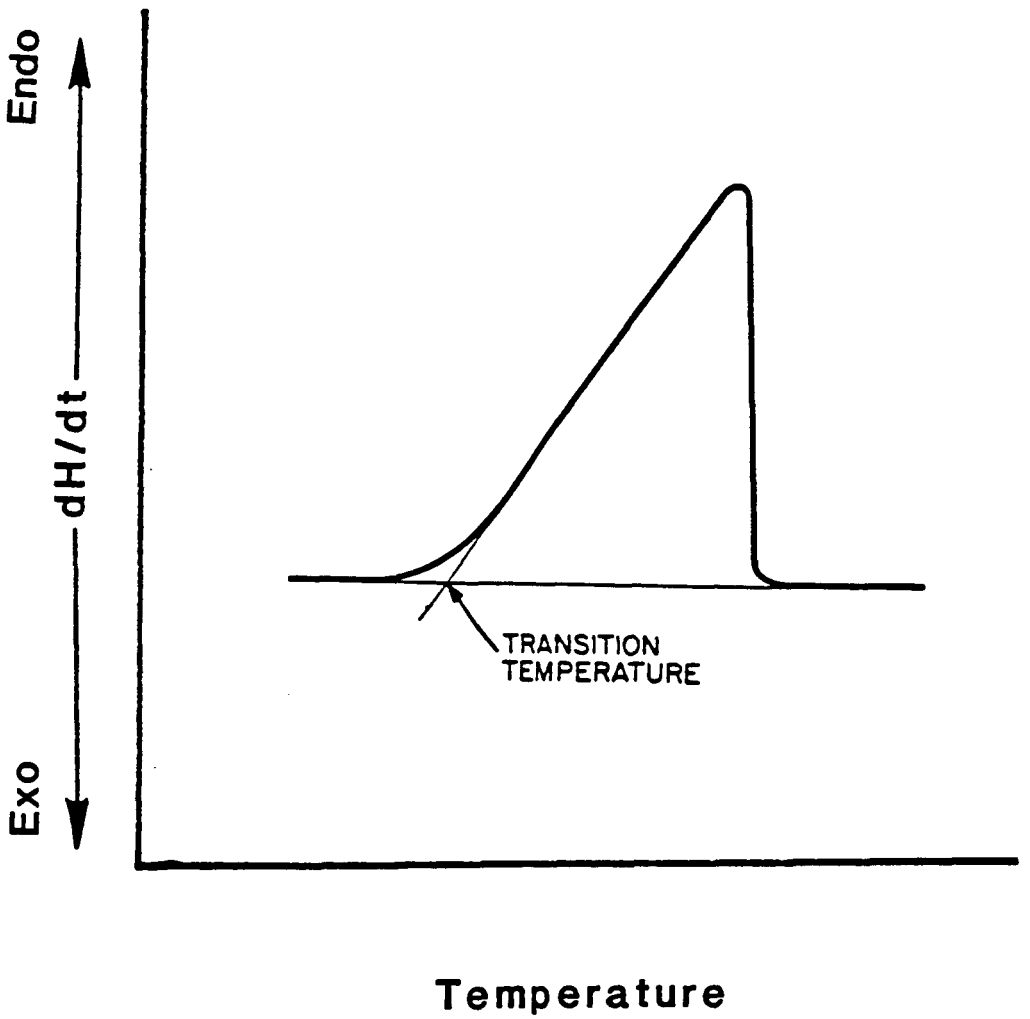

Fig. 3.1 The construction for determining transition temperature.

By means of TEMP CALIB RANGE control adjustment, the difference between ΔT_{IND} and ΔT_{ACT} can be minimized. The calibration on temperature scale is completed when $(\Delta T_{IND} - \Delta T_{ACT})$ is less than ± 0.5 K. The observed transition temperature for all the standards should be within 2 K of their actual values. A typical thermogram of K2CrO4 and Indium is shown in Fig. 3.2. In the present work, the deviation of measured temperature and actual temperature was within ± 1 K, which is quite satisfactory for our measurement.

The energy calibration involves the determination of calibration constant K and is accomplished with the ΔW BALANCE control. In practice, the measurement of energy with the Model DSC-2 will necessarily involve considerations of an instrument calibration constant, the recorder chart speed, the sensitivity used, and the unit employed for area measurement, etc. To measure the total energy associated with a transition or reaction, it is necessary to integrate over the area under the peak with respect to time

$$\Delta H = \int \frac{dH}{dt} dt \qquad (3.2)$$

The area of a peak is directly proportional to the energy of the change per unit weight, ΔH, in calories per gram, the sample weight, W and the chart speed S. It is also inversely proportional to the instrument RANGE setting, Rr. Therefore, we have

$$A = \frac{1}{K} \frac{\Delta H x W x S}{R'} \qquad (3.3)$$

where K is a proportionality constant and R' is setting RANGE of DSC. From the calibration with a standard material like Indium or Zinc through the adjustment of the ΔW calibration control, one can obtain

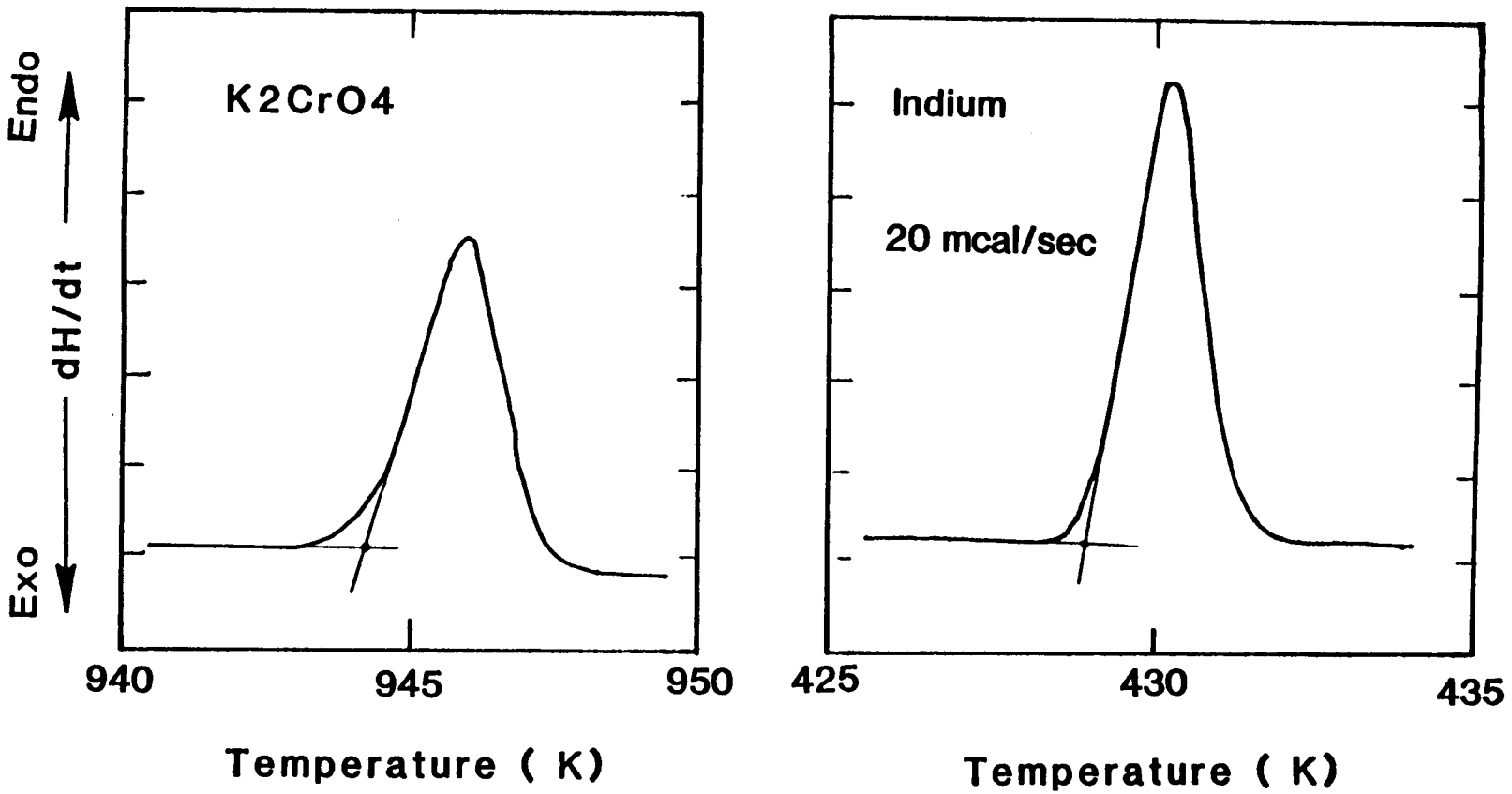

Fig. 3.2 The DSC thermograms of K2CrO4 and Indium under dynamic heating condition.

the value of K from Eq. (3.3). Table 3.1 shows the results obtained for calibration constant K used in the present work.

The baseline optimization is accomplished with SLOPE control and ΔT BALANCE control. By adjusting ΔT BALANCE and SLOPE control, the curvature and the decline of baseline could be improved until the satisfactory flatness of the baseline is obtained. Since the baseline affects the area of thermogram measured, it is recommended that the baseline optimization be conducted for different scanning conditions and materials.

3.1.4 Measurements of Degree of Cure α(t)

The degree of cure was defined as the fraction of heat released, up to time t for the resin system under cure [5] measured by Perkin-Elmer DSC-2. The measurement was made under the dynamic cure condition with a given heating rate. During the temperature scan, the rate of heat generated was recorded and plotted versus time and the area under the curve provided the amount of heat released (Fig. 3.3). The total heat of reaction, H_T, is calculated by the expression

$$H_T = \int_{t_0}^{t_f} \frac{dH}{dt}\, dt \tag{3.4}$$

where t_f is the time required to complete the reaction. The heat released up to time t, H, could also be calculated as

$$H = \int_{t_0}^{t} \frac{dH}{dt}\, dt \tag{3.5}$$

and the degree of cure can be determined by

Table 3.1 DSC calibration constant determined from the thermogram of standard material Indium (weight = 5.0 mg, ΔH = 6.8 cal/gm and heating rate = 20 K/min)

Chart. Rec. Speed sec/in.	Range mcal/sec	Area in^2	K 1/in
5	10	7.0	0.97
5	20	3.53	0.96
10	10	3.55	0.96
20	10	1.76	0.97

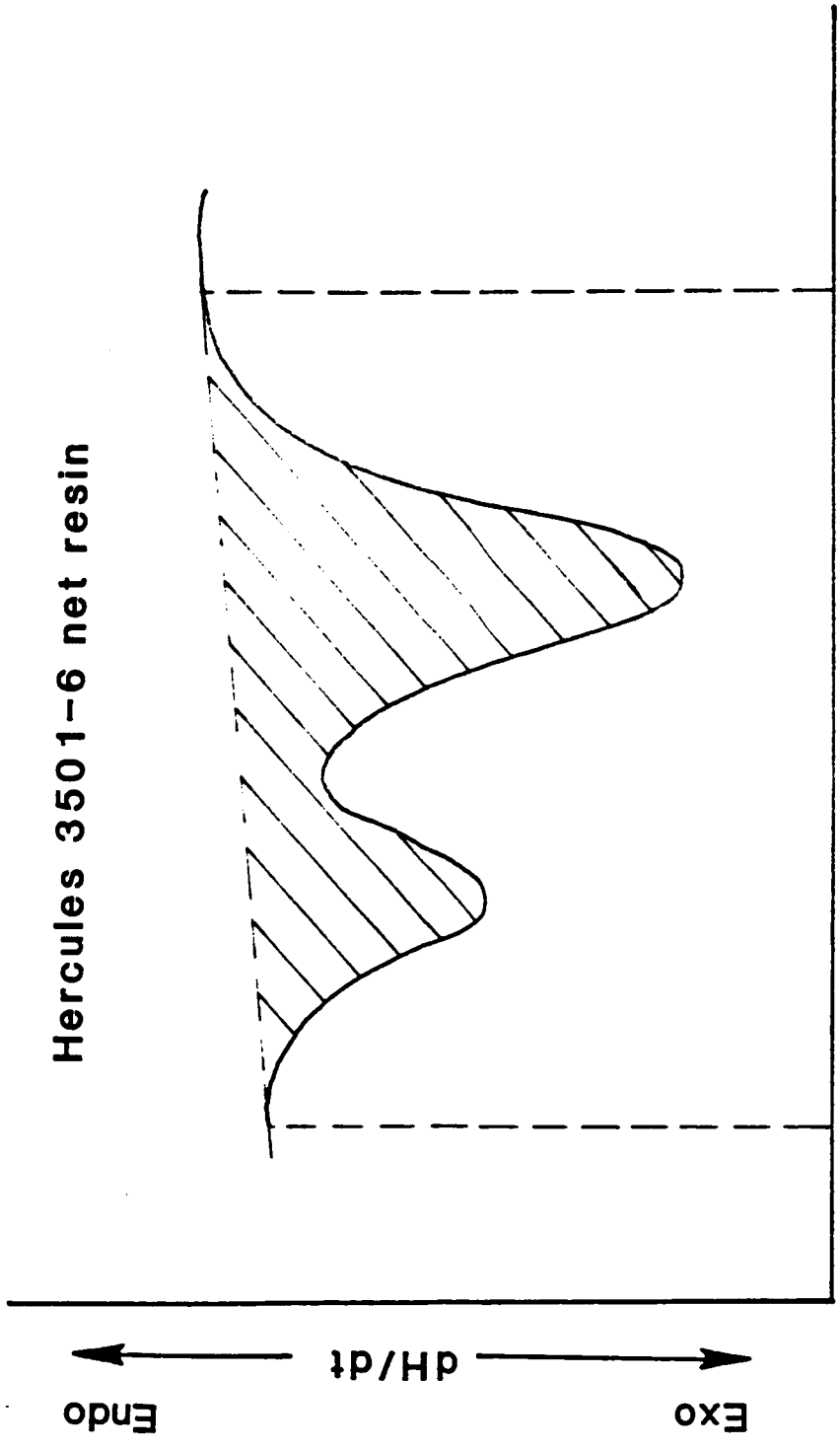

Fig. 3.3 Illustration of the DSC thermogram of Hercules 3501-6 net resin system.

$$\alpha = \frac{H}{H_T} \tag{3.6}$$

The rate or degree of cure can also be calculated by the expression

$$\frac{d\alpha}{dt} = \frac{1}{H_T}\frac{dH}{dt} \tag{3.7}$$

The measurements of degree of cure were made on Hercules 3501-6 net resin system under dynamic cure conditions according to the procedure outlined above. The heating rates were 10, 20, 40 and 80 K/min respectively. The total heat of reaction, H, is calculated by a numerical integration scheme based on Simpson's rule [11]. Experimental results are presented in Chap. 4.

3.1.5 Measurements of Glass Transition Temperature Tg(t)

Measurements of glass transition temperature under both dynamic and isothermal condition were performed. Dynamic curing experiment was performed as follows: The sample was first heated at heating rate of 20 K/min from 260 K to a specified temperature. A rapid quench to the initial temperature then followed. The resultant thermogram was obtained by re-scanning the sample at a rate of 20 K/min. A new desired temperature could be reached in this stage and subsequent measurements could be performed on the same sample. The experimental cure cycle is shown in Fig. 3.4.

In the present study, glass transition temperature at eight different states (during the advancement of the reactive resin system cured at a constant rate of heating condition of 20 K/min) were measured. The measurements were repeated for ten different samples.

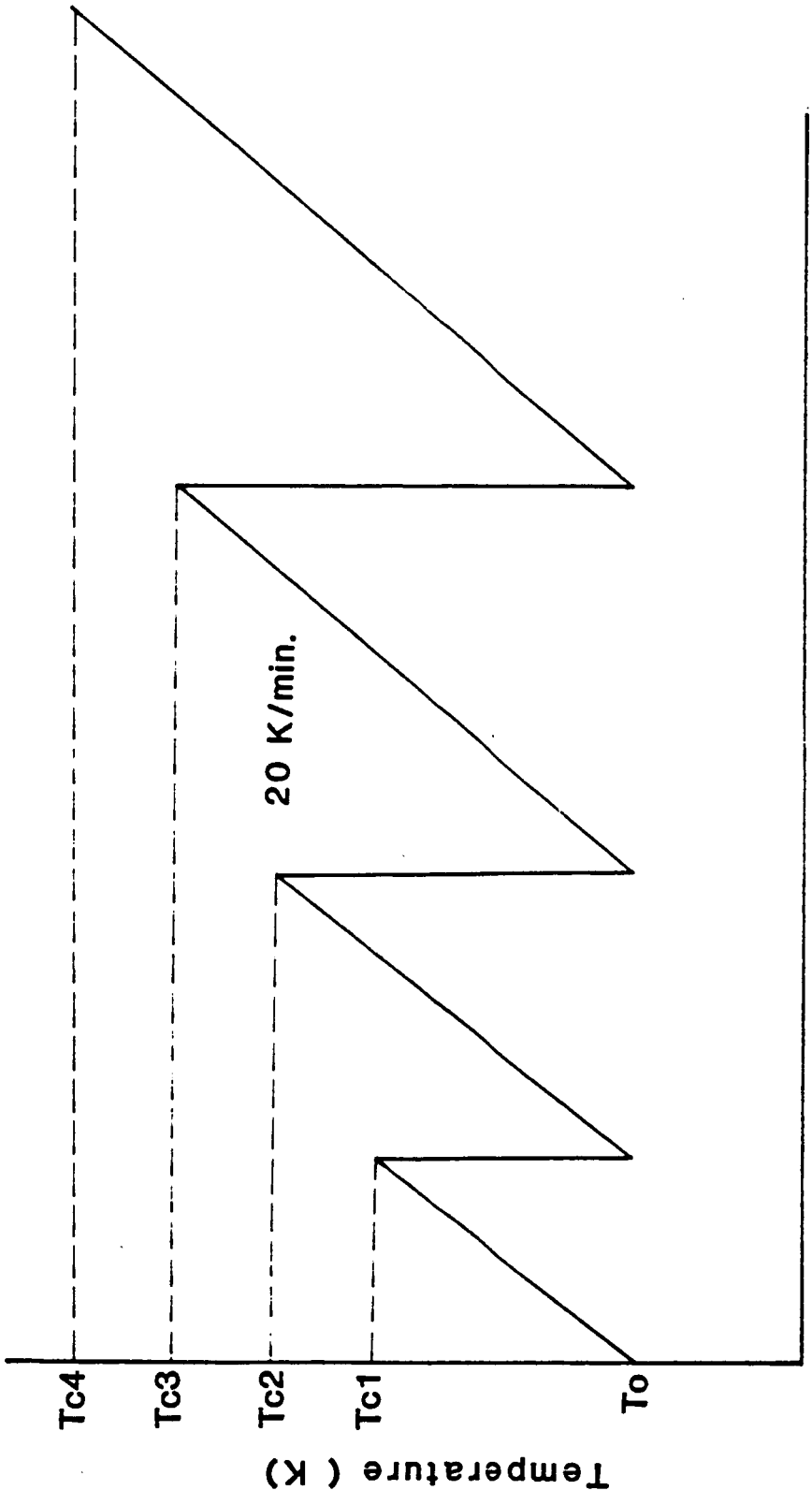

Fig. 3.4 The experimental cure cycle of glass transition temperature measurements for Hercules 3501-6 under dynamic heating condition.

In the isothermal scanning measurement, the experiment was performed as follows: The sample was first heated at a rate of 320 K/min from 260 K to a specified curing temperature. At the completion of various holding times at the temperature, a rapid quench to initial temperature followed. Subsequent thermograms were obtained by re-scanning the quenched samples at a rate of 20 K/min from 260 K to a temperature above its Tg. A number of measurements of glass transition temperature under isothermal scanning condition was conducted. The selected curing temperatures and the length of curing times were determined according to the reaction kinetics reported by Lee et al. [5].

3.2 Rheological Measurements

3.2.1 Sample Preparation

All samples were preconditioned at room temperature by pressing about 30 gm of resin between two pieces of non-porous Teflon cloth (CHR-6TB) to produce a resin wafer with a thickness of 1.25 mm. The wafers were stored in a vacuum oven for a couple of hours at a temperature of about 340 K until the volatile bubbles were no longer evident. The sample preconditioning was used to remove moisture and any other volatiles that might create erratic variations in rheology. After degasing, the sample was stored in the refrigerator and removed just prior to the experimental measurement. A disk sample was prepared by a circular puncher with a diameter of 2.50 cm.

3.2.2 Apparatus

The Rheometrics System Four [12] was used to measure the rheological properties of the material.

The Rheometrics System Four is a fully automated laboratory instrument for characterizing the rheological properties of a broad range of materials including solids, fluids and melts. It is a modular designed system of four independent servos linked to a common computer system for control and data acquisitions. These four servo motors are: Dynamic, Linear, Fluids and Steady which are selected for optimum response in their respective modes allowing a broad range of test geometrics and deformation histories.

The dynamic servo motor and a parallel plate test geometry are selected in the present study to measure chemoviscosity of the reaction epoxy resin system. Sample temperature is controlled with a convected gas environmental chamber. The torque and normal force generated in response to the imposed motion is measured by the transducer. The computer calculates stresses from the torque and normal force measurements and combines these values with measured sample deformation to calculate values of the selected rheological properties. The computer and associated electronics also provide precision control and rapid data analysis with results conveniently printed out in graphical and tabular forms.

In measuring chemoviscosity of Hercules 3501-6 epoxy resin, a time sweep mode or cure mode were selected respectively in isothermal or dynamic cure condition.

3.2.3 Calibration

The calibration of Rheometrics includes: transducer normal and torque calibration, temperature calibration and phase calibration.

Transducer calibration must be performed whenever a transducer is changed. Periodic calibration checks should be performed to ensure the accuracy of test results. Calibration is accomplished through adjustment of normal calibration control and torque control by comparing measured data with standard weight.

The phase calibration is accomplished to compensate for phase shift in the electronics through the adjustment of appropriate potentiometer. Calibration was performed with the dynamic motor in TORSION RECT using an elastic material such as steel which possesses a phase angle of zero degrees and a low viscosity newtonian fluid which possesses a phase angle of -90 degrees. Calibration in TORSION RECT or BENDING with a material such as steel is the preferred method as the phase angle of steel is not frequency or strain dependent. For newtonian fluids and elastic samples, the tolerance is -0.4 and -0.25 degrees respectively.

3.2.4 Measurement of Chemoviscosity

The chemoviscosity data under isothermal condition has been measured previously [13]. The selected temperatures were 360, 375, 385, 399, 410, 425 and 435 K.

The measurement of chemoviscosity in a dynamic case was conducted in present study. During the measurement, the sample was confined to the gap between two parallel plates mounted in the Rheometer. The top plate was motor driven about its axis while the bottom plate was mounted

on a torque transducer for force measurement. The typical gap between the parallel plates was 1.2 mm. The plates and sample were enclosed in a heating chamber where temperature control was provided. Selection of the strain value was to assure that the measurements were performed within the material's linear viscoelastic response range.

It is well known that the viscoelastic properties of polymeric materials respond differently to different frequencies, and selection of the frequency value was made to assure that the complex viscosities measured were within the Newtonian region [12]. The cure mode of the Rheometer was used during testing which automatically programmed different temperature profiles as the epoxy was cured.

The sample was first kept at 300 K for about 5 minutes before measurement started. Experimental measurements were performed under different rates of heating conditions.

Chapter 4

EXPERIMENTAL RESULTS

4.1 Material

The material used in the study is Hercules 3501-6 net epoxy resin. This thermosetting system was selected because of its wide use in aerospace industry. The material received from the manufacturer was used without further treatment, and was kept in the dark and cold conditions at around -5°C.

The material contains the following standard concentrations of starting components [14]:

COMPONENT	TOTAL PERCENT (wt)
Tegraglycidyl Methylenedianiline	56.5
Alicyclic Diepoxy Carboxylate	9.0
Epoxy Cresol Novalac	8.5
4,4' Diaminodiphenyl Sulfone	25.0
Boron Trifluoride Amine Complex	1.1

4.2 Experimental Data of Thermal Analysis

4.2.1 Degree of Cure $\alpha(t)$

4.2.1.1 Isothermal Case. Lee et al. [5] performed thermal analyses on the same epoxy resin system by DSC. The degree of cure α and the rate of change of degree of cure $d\alpha/dt$ were determined from

the results of the isothermal scanning experiments. Eight different temperatures were selected, and the results are reproduced in Fig. 4.1. It is noted from the figure that both higher values of the degree of cure and rate of change of degree of cure are decreasing functions of cure time t, and eventually level off at a low value (< 0.1) when a high degree of cure is reached. The following equations were found to describe the temperature-dependent data rather accurately:

$$d\alpha/dt = (K_{n_1} + K_{n_2}\alpha)(1-\alpha)(B-\alpha) \qquad \alpha < 0.3 \qquad (4.1a)$$

$$d\alpha/dt = K_{n_3}(1-\alpha) \qquad > 0.3 \qquad (4.1b)$$

where

$$K_{n_1} = A_1 \exp(-\Delta E1/RT)$$

$$K_{n_2} = A_2 \exp(-\Delta E2/RT)$$

$$K_{n_3} = A_3 \exp(-\Delta E3/RT)$$

The values of constants in Eqs. (4.1a) and (4.1b) are summarized in Table 4.1. Comparisons between the measured values of $d\alpha/dt$ and the values calculated by Eqs. (4.1a) and (4.1b) are also shown in Fig. 4.1 by symbols and solid lines respectively.

4.2.1.2 Dynamic Case. The measurements of heat of reaction and degree of cure under dynamic heating condition were performed with four different heating rates, 10, 20, 40 and 80 K/min respectively. A typical thermogram at 20 K/min is shown in Fig. 4.2. It is seen that there are two "humps" in the curve. These humps are caused by two different major reactions occurring during the cure. The total heat of

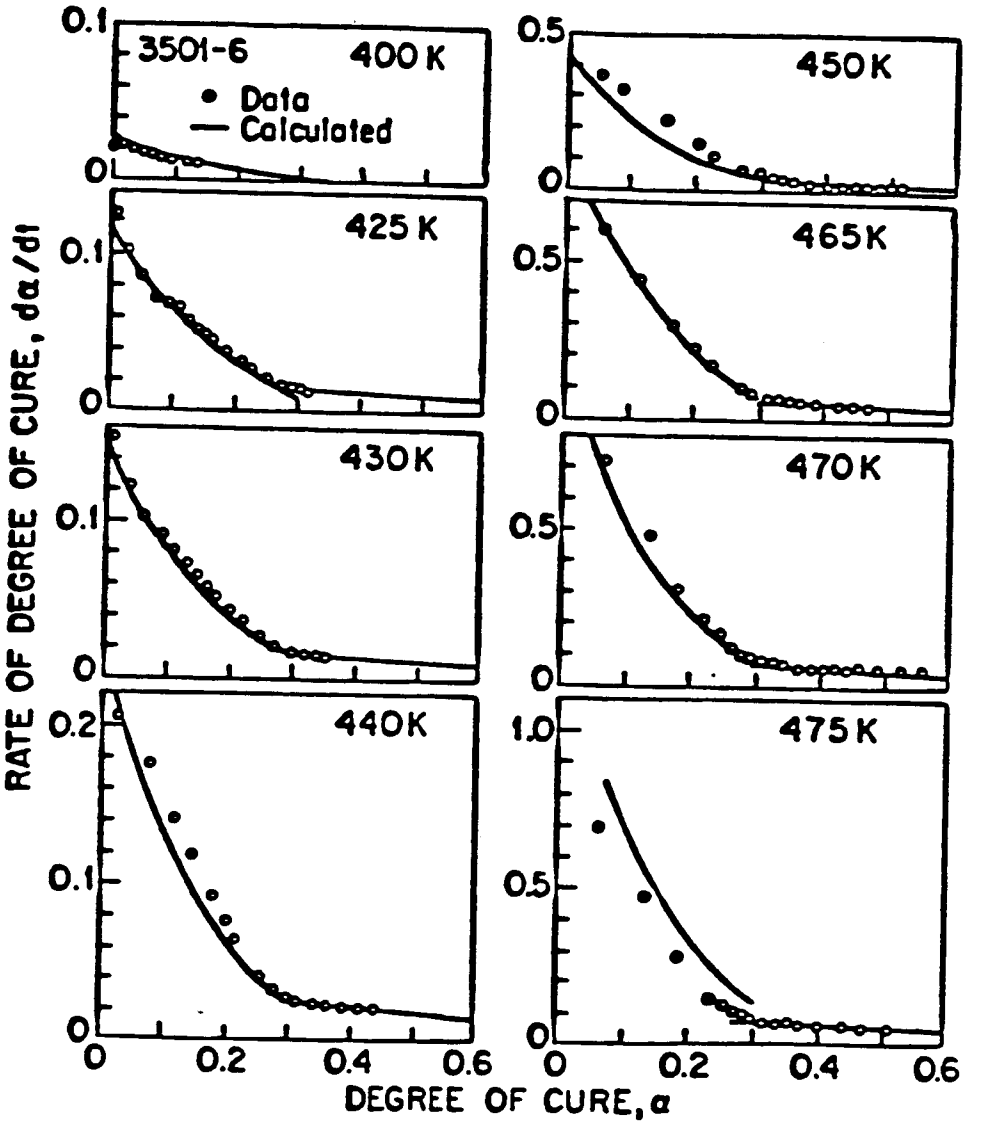

Fig. 4.1 Rate of degree of curve vs. degree of cure reported by Lee, Loos and Springer [5] for Hercules 3501-6 resin system under isothermal cure cycles; solid lines were calculated using Eqs. (4.1a) and (4.1b).

Table 4.1 Values of constants Eqs. (4.1a) and (4.1b) for Hercules 3501-6 resin system under isothermal condition

$B = 0.47$
$A_1 = 2.101 \times 10^9 \text{ min}^{-1}$
$A_2 = -2.014 \times 10^9 \text{ min}^{-1}$
$A_3 = 1.960 \times 10^5 \text{ min}^{-1}$
$\Delta E_1 = 8.07 \times 10^4 \text{ J/mole}$
$\Delta E_2 = 7.78 \times 10^4 \text{ J/mole}$
$\Delta E_3 = 5.66 \times 10^4 \text{ J/mole}$

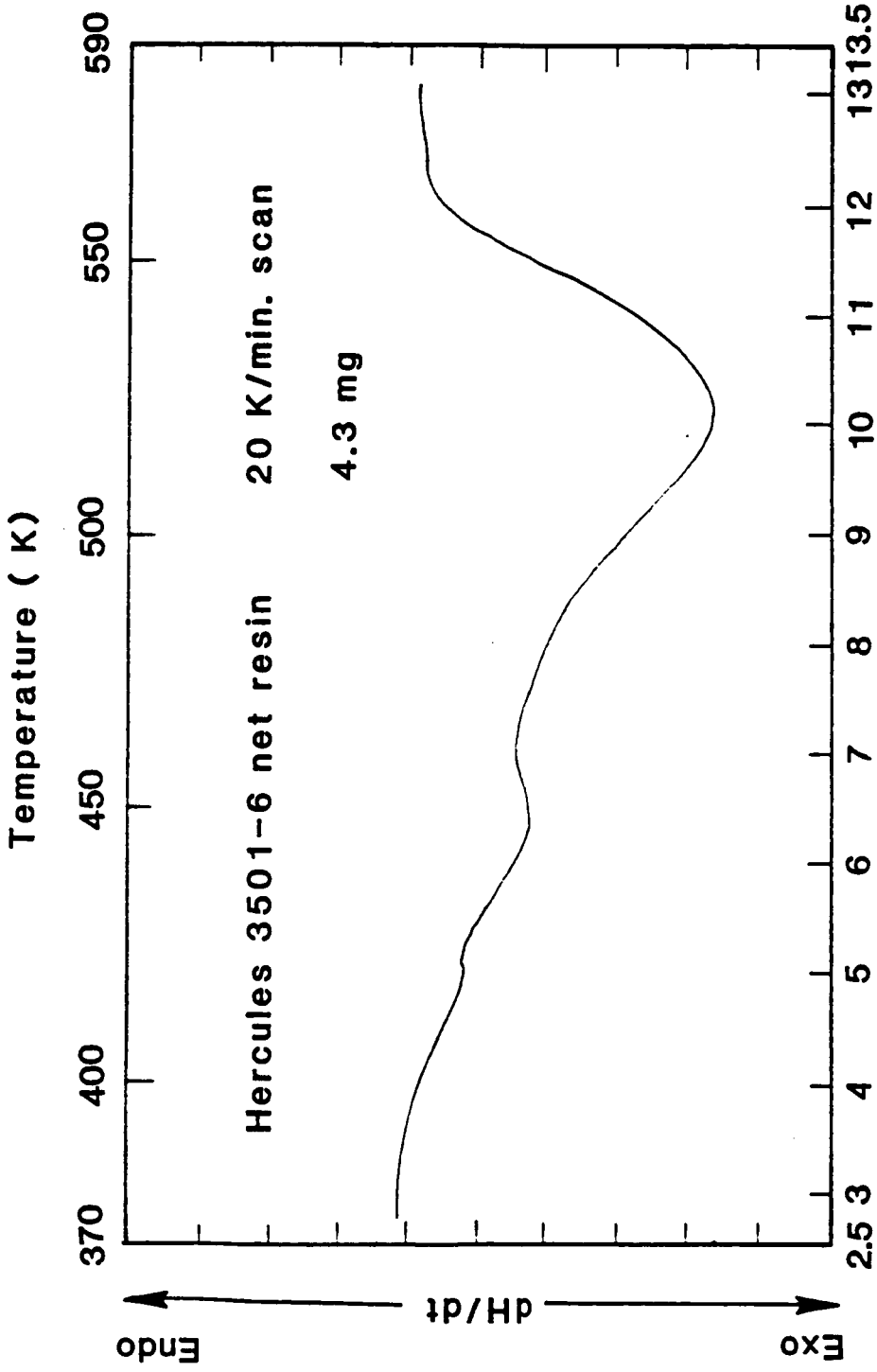

Fig. 4.2 A typical rate of heat generation vs. time curve of Hercules 3501-6 resin system provided by dynamic scanning experiments under 20 K/min rate of heating condition.

reaction H was calculated by numerical integration according to the Simpson's rule. The algorithm was programmed in FORTRAN and was run by a VAX computer system. Program codings are included in Appendix B for references. Calculated results are tabulated in Table 4.2. It can be seen that H_T is independent of heating rates. An average value of H_t = 120±5.0 cal/gm was chosen to be used in all future calculations. The total heat of reaction calculated by Lee et al. [5] in dynamic scanning experiment was 113.4 cal/gm. A ten percent difference between the two results is noted. This is possibly caused by materials with different aging histories and the scheme employed in determining thermogram and the area under the peak of the curve.

The degree of cure $\alpha(t)$ was also calculated based on the thermograms. The results are plotted in Fig. 4.3. Open and filled symbols represent results from different runs under the same condition. The reproducibility of the measurements appears to be very satisfactory. Numerical solution of Eqs. (4.1a) and (4.1b) under dynamic heating condition where temperature was not kept constant is outlined as follows.

In a dynamic heating case, reacting kinetics of resin system becomes a first-order, non-linear and initial-value differential equation, i.e.,

$$\frac{\partial \alpha}{\partial t} = f(t, \alpha) \quad , \quad \alpha(t_o) = \alpha_o \tag{4.2}$$

Assume that f is sufficiently differentiable with respect to either t or α. It is known [15] that Eq. (4.2) possesses a unique solution if $\frac{\partial f}{\partial \alpha}$ is continuous on the interval of interest. If $\alpha(t)$ is the exact solution of Eq. (4.2), then we can expand $\alpha(t)$ in a Taylor series about the point $t = t_o$ as

Table 4.2 Total heat of reaction for Hercules 3501-6 resin system measured at different rate of heating conditions

Weight mg	Rate °K/min.	Heating Speed sec/in.	Chart. Rec. Range mcal/sec	H_T cal/gm
4.6	10	60	0.5	118.702
5.5	10	60	0.5	120.129
6.4	10	60	0.5	126.472
5.2	20	40	0.5	119.474
6.7	20	40	0.5	119.474
5.7	40	20	1.0	125.37
7.6	80	10	2.0	118.34
5.3	80	10	2.0	118.32

Heating Rate (°K/min)	Ave. $\bar{H}_T$ (cal/gm)
10	121.77 ± 4.136
20	122.39 ± 4.131
40	120.02 ± 6.26
80	118.3 ± 2.21

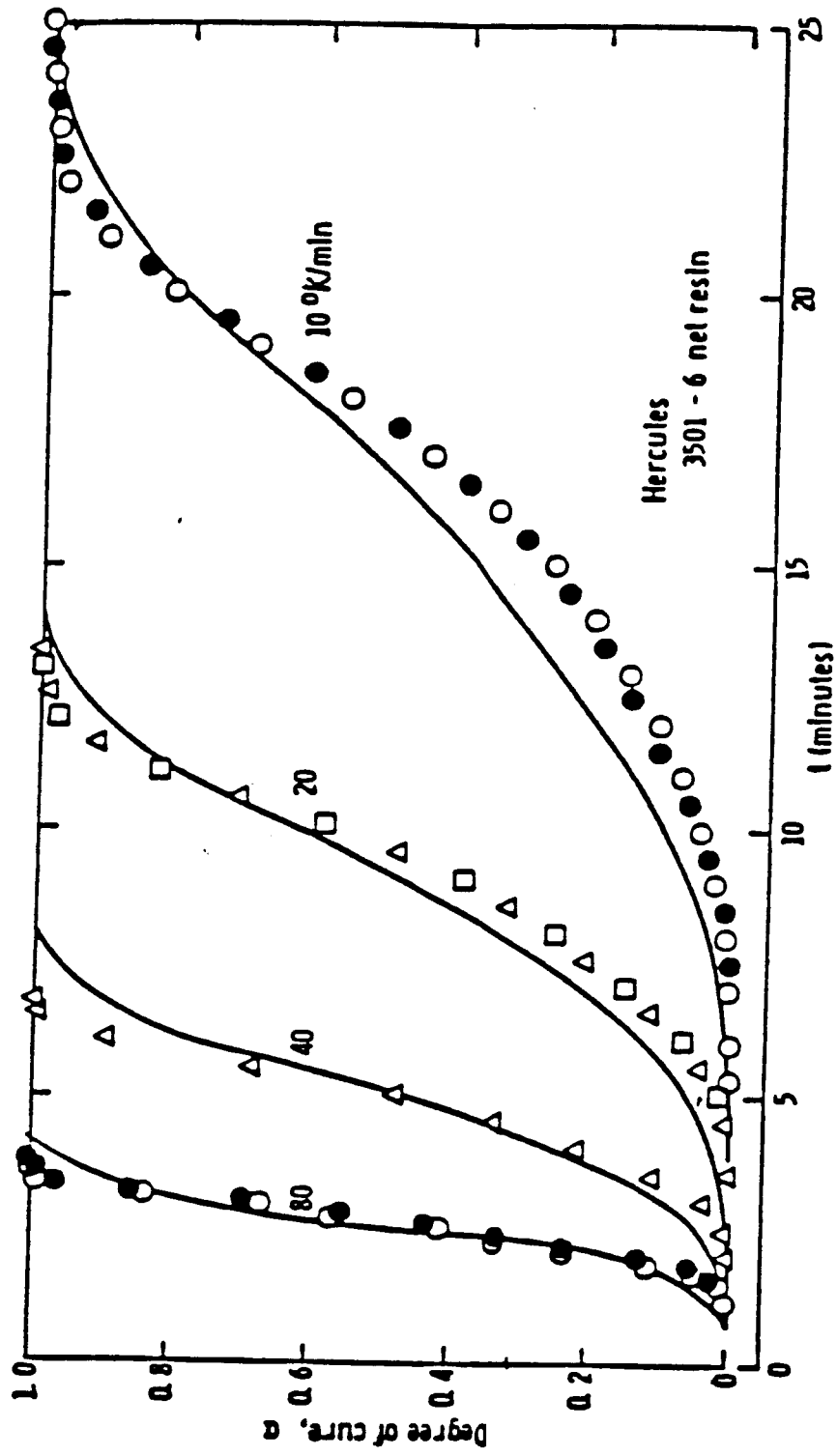

Fig. 4.3 Degree of cure α(t) measured for Hercules 3501-6 resin system cured under four different rates of heating condition shown.

$$\alpha(t) = \alpha_o + (t - t_o) \frac{\partial\, \alpha(t_o)}{\partial t} + \frac{(t - t_o)^2}{2!} \frac{\partial^2\, \alpha(t_o)}{\partial t^2} \tag{4.3}$$

By taking the total derivative of Eq. (4.2) with respect to t, (keeping in mind that f is an implicit function of α), we have

$$\frac{\partial \alpha}{\partial t} = f(t, \alpha) \tag{4.4}$$

$$\frac{\partial^2 \alpha}{\partial t^2} = f' = \frac{\partial f}{\partial t} + \frac{\partial f}{\partial \alpha} \frac{\partial \alpha}{\partial t} \tag{4.5}$$

For $\alpha < 0.3$:

$$f(t, \alpha) = (K_{n_1} + K_{n_2}\, \alpha)\, (1 - \alpha)\, (B - \alpha) \tag{4.6}$$

$$\frac{\partial f}{\partial t} = \frac{\Delta E_1}{Rkt^2} \left(K_{n_1} + \frac{\Delta E_2}{\Delta E_1} K_{n_2}\, \alpha\right) (1 - \alpha)\, (B - \alpha) \tag{4.7}$$

$$\frac{\partial f}{\partial \alpha} = K_{n_2}\, (1 - \alpha)\, (B - \alpha) - (K_{n_1} + K_{n_2}\, \alpha)\, (B - \alpha) - (K_{n_1} + K_{n_2}\, \alpha)\, (1 - \alpha) \tag{4.8}$$

For $\alpha > 0.3$:

$$f(t, \alpha) = A_3 e^{-\frac{\Delta E_3}{Rkt}} (1 - \alpha) = K_{n_3}\, (1 - \alpha) \tag{4.9}$$

$$\frac{\partial f}{\partial t} = \frac{\Delta E_3}{Rkt^2} K_{n_3}\, (1 - \alpha) \tag{4.10}$$

$$\frac{\partial f}{\partial \alpha} = - K_{n_3} \tag{4.11}$$

By denoting $\alpha(t_i) = \alpha_i$, we have

$$\alpha_{i+1} = \alpha_i + \Delta t_i \frac{\partial \alpha_i}{\partial t} + \frac{\Delta t_i^2}{2!} \frac{\partial^2 \alpha_i}{\partial t^2} \tag{4.12}$$

$$\alpha(t_o) = \alpha(0) = 0$$

where $i = 0, 1, 2, 3, \ldots$, and

$$\frac{\partial \alpha_i}{\partial t} = (K_{n_1} + K_{n_2}\,\alpha_i)\,(1 - \alpha_i)\,(B - \alpha_i) \qquad \alpha < 0.3 \qquad (4.13a)$$

$$\frac{\partial \alpha_i}{\partial t} = K_{n_3}\,(1 - \alpha_i) \qquad \alpha > 0.3 \qquad (4.13b)$$

$$\frac{\partial^2 \alpha_i}{\partial t^2} = \frac{\Delta E_1}{Rkt}\,(K_{n_1} + \frac{\Delta E_2}{\Delta E_1}\,K_{n_2}\,\alpha_i)\,(1 - \alpha_i)\,(B - \alpha_i) + [K_{n_2}(1 - \alpha_i)(B - \alpha_i)$$

$$- (K_{n_1} + K_{n_2}\,\alpha_i)\,(B - \alpha_i) - (K_{n_1} + K_{n_2}\,\alpha_i)\,(1 - \alpha_i)]\,[(K_{n_1}$$

$$+ K_{n_2}\,\alpha_i)\,(1 - \alpha_i)\,(B - \alpha_i)] \qquad \alpha < 0.3 \qquad (4.14a)$$

$$\frac{\partial^2 \alpha_i}{\partial t^2} = \frac{\Delta E_3}{Rkt^2}\,K_{n_3}\,(1 - \alpha_i) - K_{n_3}^2\,(1 - \alpha_i) \qquad \alpha > 0.3 \qquad (4.14b)$$

The numerical results are plotted by solid curves in Fig. 4.3. Considering the fact that the temperature ranges of 400 to 475 K covered by isothermal experiments, as represented by Eqs. (4.1a) and (4.1b), is narrower than the ranges of 320 to 600 K covered here by the dynamic heating experiments, the agreements shown in the figure are rather satisfactorily. Figure 4.3 also implies that information such as chemoviscosity $\eta(t)$ and degree of cure $\alpha(t)$ under dynamic heating cure conditions can be related within certain accuracy to those obtained under isothermal curing conditions.

4.2.2 Glass Transition Temperature Tg(t)

4.2.2.1 Isothermal Case. It was found that the major reaction of material occurred within the range of 420 to 500 K in dynamic curing condition. The range of degree of cure was between 0.1 and 0.5. It is the range in which the simulations of the chemoviscosity-time profiles are performed.

The glass transition temperature Tg(t) was determined for isothermal curing conditions at five temperatures of 430, 440, 450, 460 and 480 K respectively. A set of three degrees of cure was selected for each curing temperature as shown in Table 4.3. The corresponding set of curing time, t, was determined by solving Eqs. (4.1a) and (4.1b) isothermally, and this is presented by

$$t = \frac{a}{K_{n_2}} \ln\left(1 + \frac{K_{n_2}}{K_{n_1}} \alpha\right) - b \ln(1-\alpha) - c \ln\left(1 - \frac{\alpha}{B}\right) \quad \alpha < 0.3 \qquad (4.15a)$$

$$t = \frac{1}{K_{n_3}} \ln\left(\frac{1-\alpha}{0.7}\right) + tc \quad \alpha > 0.3 \qquad (4.15b)$$

where

$$a = K_{n_2}^2 (B-1)/d$$

$$b = (K_{n_1} + K_{n_2} B)/d$$

$$c = -(K_{n_1} + K_{n_2})/d$$

$$d = (K_{n_1} + K_{n_2}) \{K_{n_2} B^2 + (K_{n_1} - K_{n_2}) B - K_{n_1}\}$$

and tc is the time given by Eq. 4.4a for $\alpha = 0.3$. The selected curing temperatures and the length of curing times for isothermal measurements are tabulated in Table 4.3.

Table 4.3 Glass transition temperature measured for Hercules 3501-6 resin system during five isothermal curing conditions

Curing Temp. (K)	Curing Time (min.)	Degree of Cure	Class Trans. Temp. (K)
430	0.85	0.1	298.0
	2.53	0.2	304.25
	6.73	0.3	313.75
440	0.67	0.12	300,25
	1.82	0.22	306.25
	4.73	0.32	316.88
450	0.55	0.15	307.0
	1.47	0.25	316.25
	3.78	0.35	325.25
460	0.92	0.25	318.0
	2.48	0.35	329.5
	4.75	0.45	343.75
480	1.3	0.35	338.3
	2.37	0.45	361.75
	3.83	0.55	385.3

A set of typical traces obtained from isothermal measurements is shown in Fig. 4.4. During the glass transition, the material undergoes a transition from glassy state to rubbery state, and the specific heat Cp of the material is changed. Thus, a step change is observed in the thermogram. Tg is determined at the arrow marks shown in the curve. The data obtained from the measurements is listed in Table 4.3.

It is found that the glass transition temperature in isothermal curing condition depends not only on the degree of cure (or curing time), but also the curing temperature. A plot of Tg vs. α at various curing temperatures is given in Fig. 4.5. The data was fitted by linear Least Square technique. The relationship between glass transition temperature and degree of cure can be expressed as

$$Tg = d1(T)\ \alpha(t) + d2 \qquad (4.16)$$

where d1 is a temperature dependent parameter.

An Arrhenius type plot of d1 vs. 1/T is shown in Fig. 4.6. By means of linear Least Square fit, two straight lines are represented, respectively, by

$$Logd1(T) = -639.56/T + 3.357 \qquad T < 450\ K \qquad (4.17a)$$

$$Logd1(T) = -3216.49/T + 8.879 \qquad T > 450\ K \qquad (4.17b)$$

The correlating factors of the above two linear fits are 0.999.

4.2.2.2 Dynamic Case. The glass transition temperatures for the material at twelve different states during cure at a constant rate of heating condition of 20 K/min were measured. The measurements were repeated for ten different samples. The method of determination of Tg

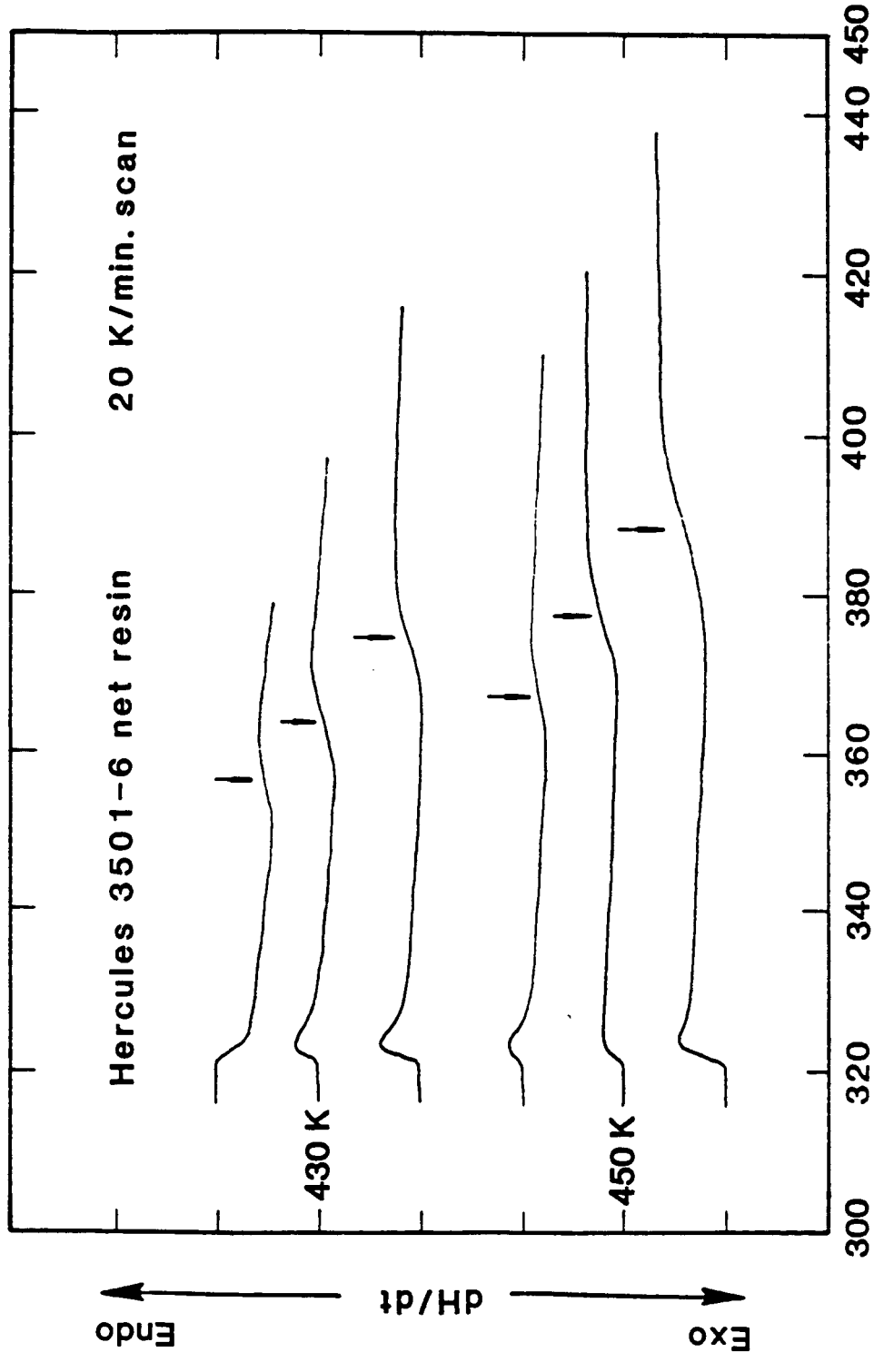

Fig. 4.4 The typical thermogram of glass transition of Hercules 3501-6 resin system under isothermal cure condition; the curing temperatures are 430 and 450 K respectively.

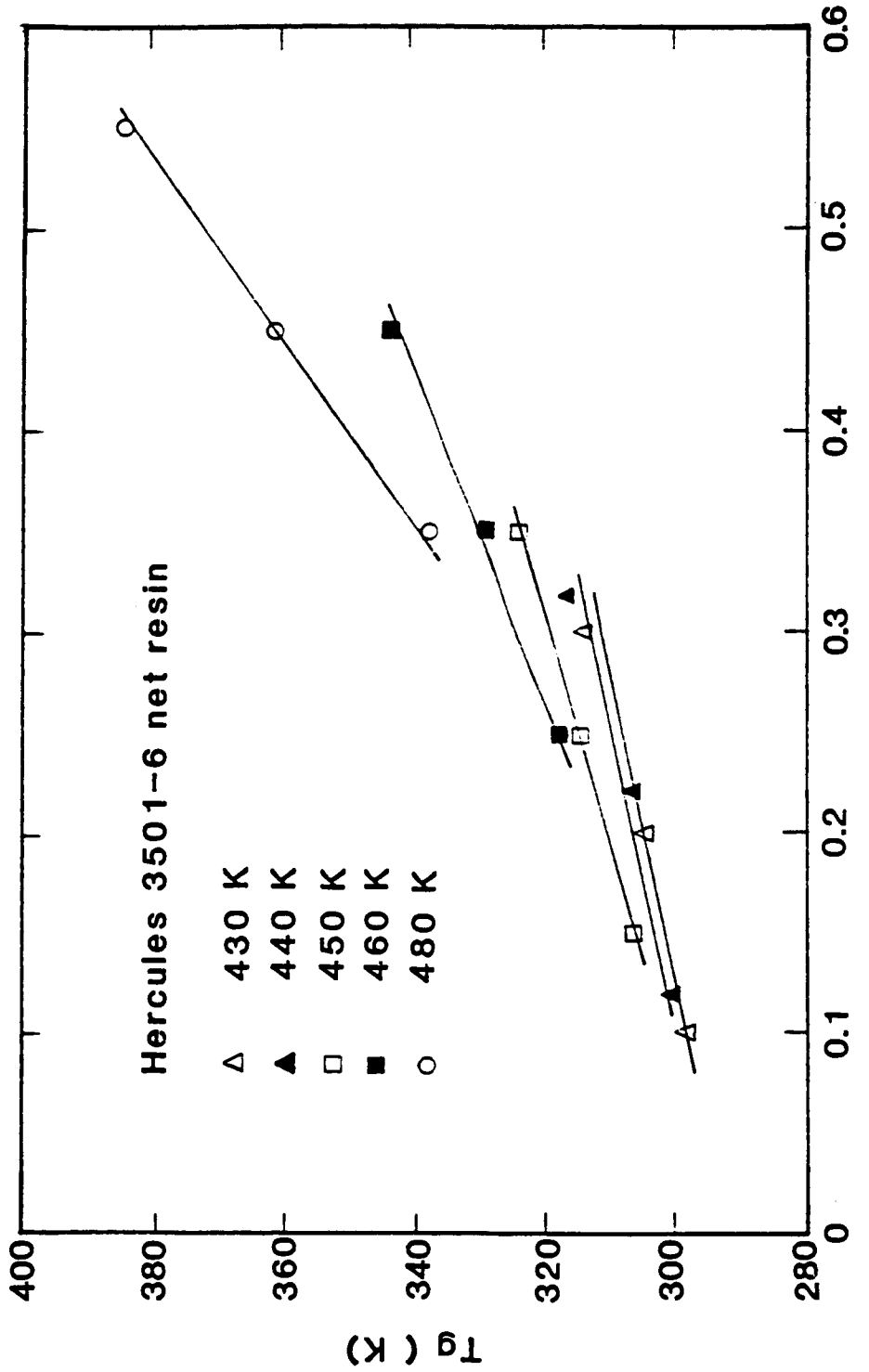

Fig. 4.5 The glass transition temperature Tg as a function of degree of cure for Hercules 3501-6 resin system under different isothermal curing temperatures shown.

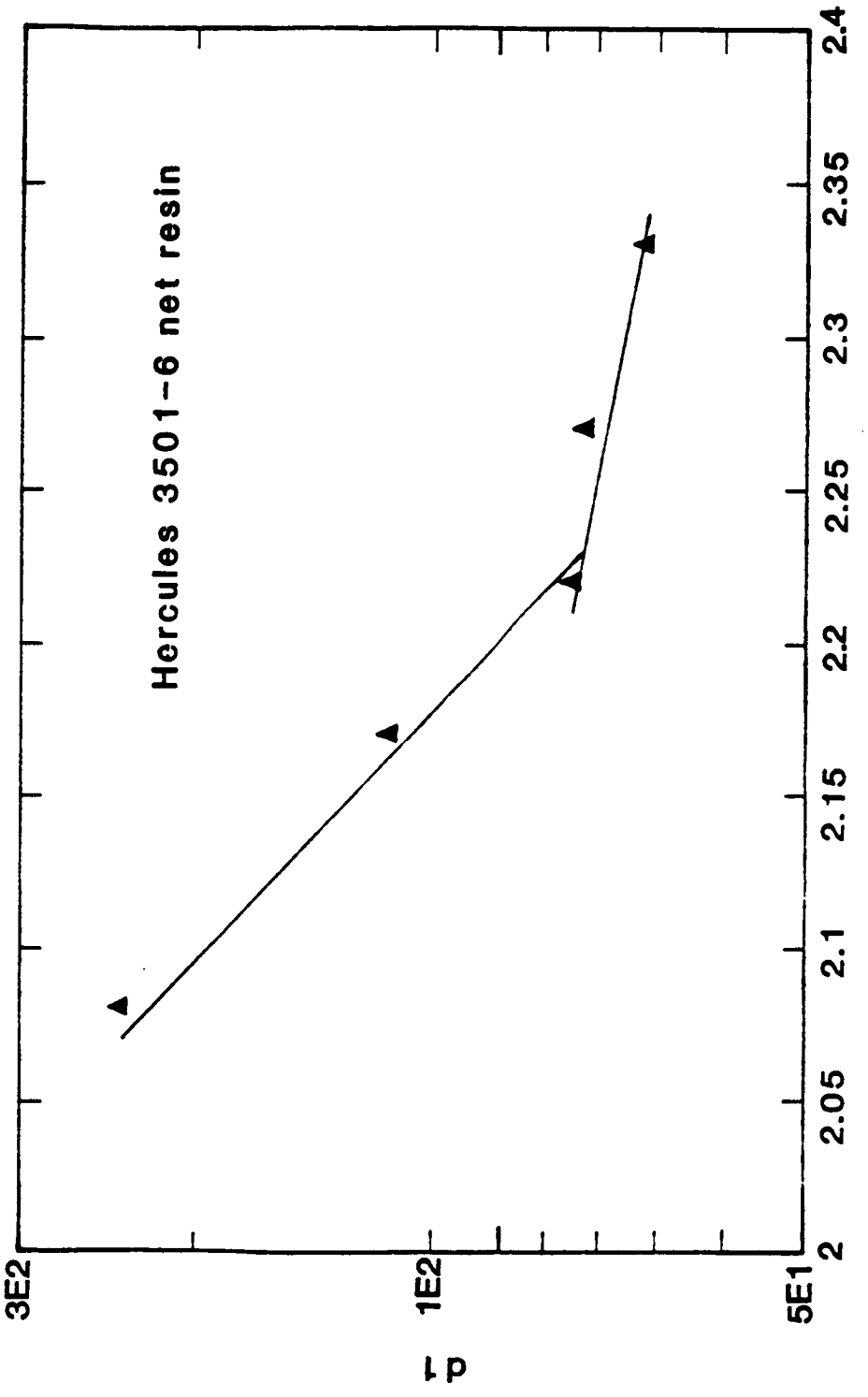

Fig. 4.6 Plots of temperature dependent parameter of Eq. (4.5) d1(T) vs. 1/T for Hercules 3501-6 resin system under isothermal curing conditions.

from the trace was the same as that in the isothermal case. The measured results are tabulated in Table 4.4 together with degree of cure $\alpha(t)$ measured by the procedures outlined above. Average values of Tg(t) and standard deviation at different resin states defined by curing time t (or curing temperature T) are included as well. It is noted that standard deviations increase for increasing scanning temperatures. Difficulties in determining Tg accurately come from two sources: (i) the higher the scanning temperatures, the less sharpness for the step change of dH/dt at the glass transition temperature and (ii) the existence of baseline slope which is usually distorted at higher temperature regimes. Nevertheless, a 90% confidence level can be achieved with ± 3% of the experimentally determined values of Tg(t).

Values of Tg(t) are plotted in Fig. 4.7. For the dynamic case, cure cycle T(t) = 20t with a constant heating rate of 20 K/min is substituted into Eq. (4.3), the glass transition temperatures in dynamic heating condition can then be calculated from the formulas for the isothermal case. Comparisons between the calculated values (the solid curve) and experimental data are shown in Fig. 4.7. Favorable comparisons are seen for the changes of the glass transition temperature in dynamic heating case below 0.5 degree of cure, where the simulations of the chemoviscosity-time profiles are performed.

4.3 Experimental Data of Rheological Measurement

4.3.1 Isothermal Case

The chemoviscosity results obtained for isothermal conditions are shown in Fig. 4.8. The curing temperatures are 360, 375, 385, 399, 410, 425 and 435 K. It is noted that for a higher cure temperature, a

Table 4.4 Glass transition temperature measured during reaction advancement of Hercules 3501-6 resin system under 20 K/min rate of heating condition

Cure Temp at the end T_e(°K)	320	400	425	450	475	500	510	525
Degree of Cure α	0	0.0001	0.03	0.11	0.23	0.399	0.49	0.645
JMB061485-1	284	288		310		356.7		425.3
JMB061785-1	285.3	288		310.6		352		430.7
JMB061885-1	283.3	287.3		306.7		364		426
JMB061985-1	283.3	286		309.3		353		411.3
JMB062085-1	282.6			304.7		348.7		418
JMB061785-2	285.3		294		324	382		
JMB061885-2	284.3		294.7		328	378		
JMB061885-3	284.7		298.7		320.7	378		
JMB061985-2	283.3		295.3		323.3	371.3		
JMB062085-2	283.3		292		321.3	380.7		
Tg	283.94	287.33	294.9	308.3	323.47	354.88	378	422.26
$\left[\frac{\Sigma(\Delta T_g)^2}{n=1}\right]^{\frac{1}{2}} = \sigma$	0.934	0.943	2.442	2.485	2.002	3.899	4.129	6.318

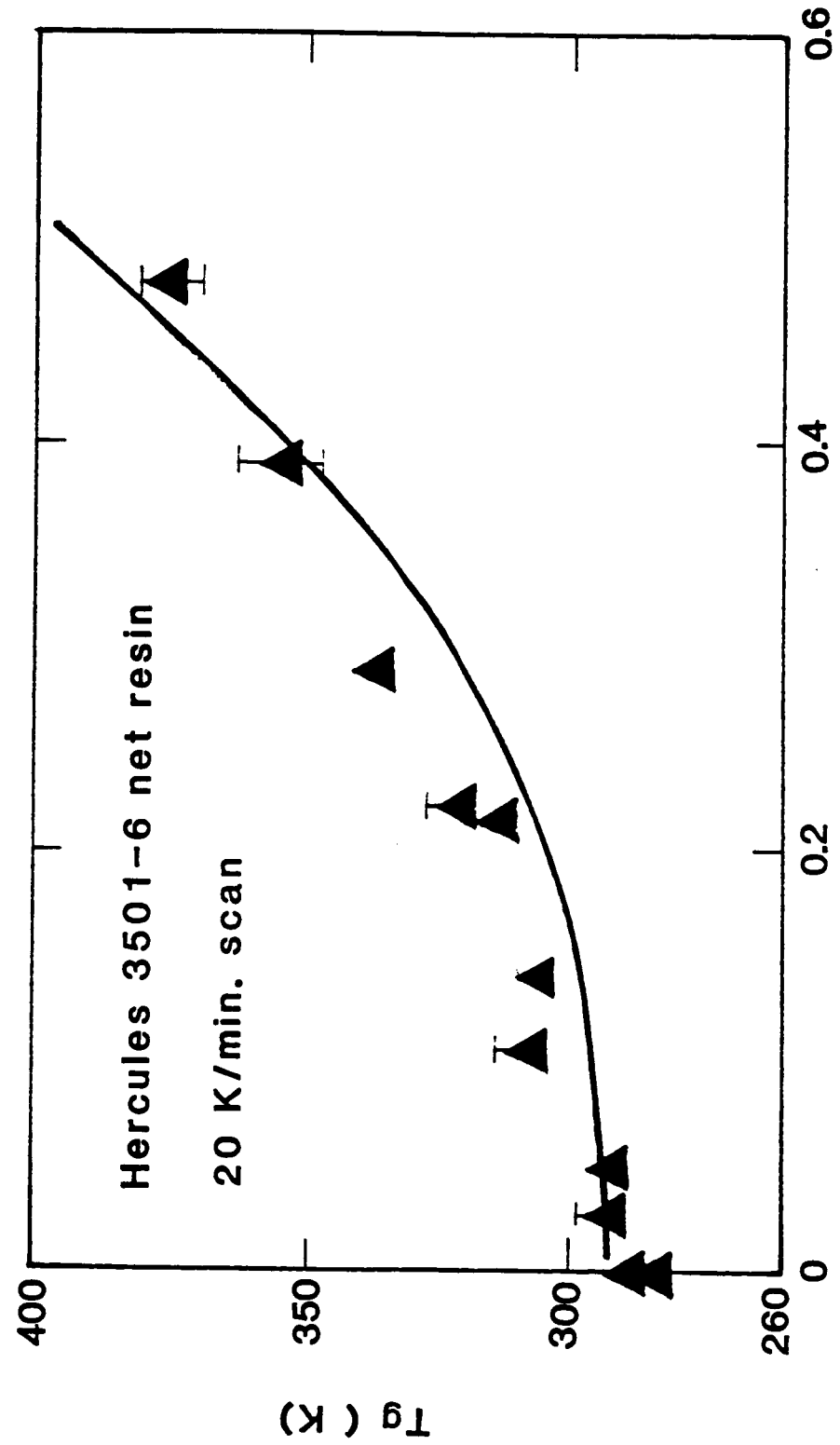

Fig. 4.7 Plot of Tg(t) vs. α(t) for Hercules 3501-6 resin system under dynamic heating condition at 20 K/min.

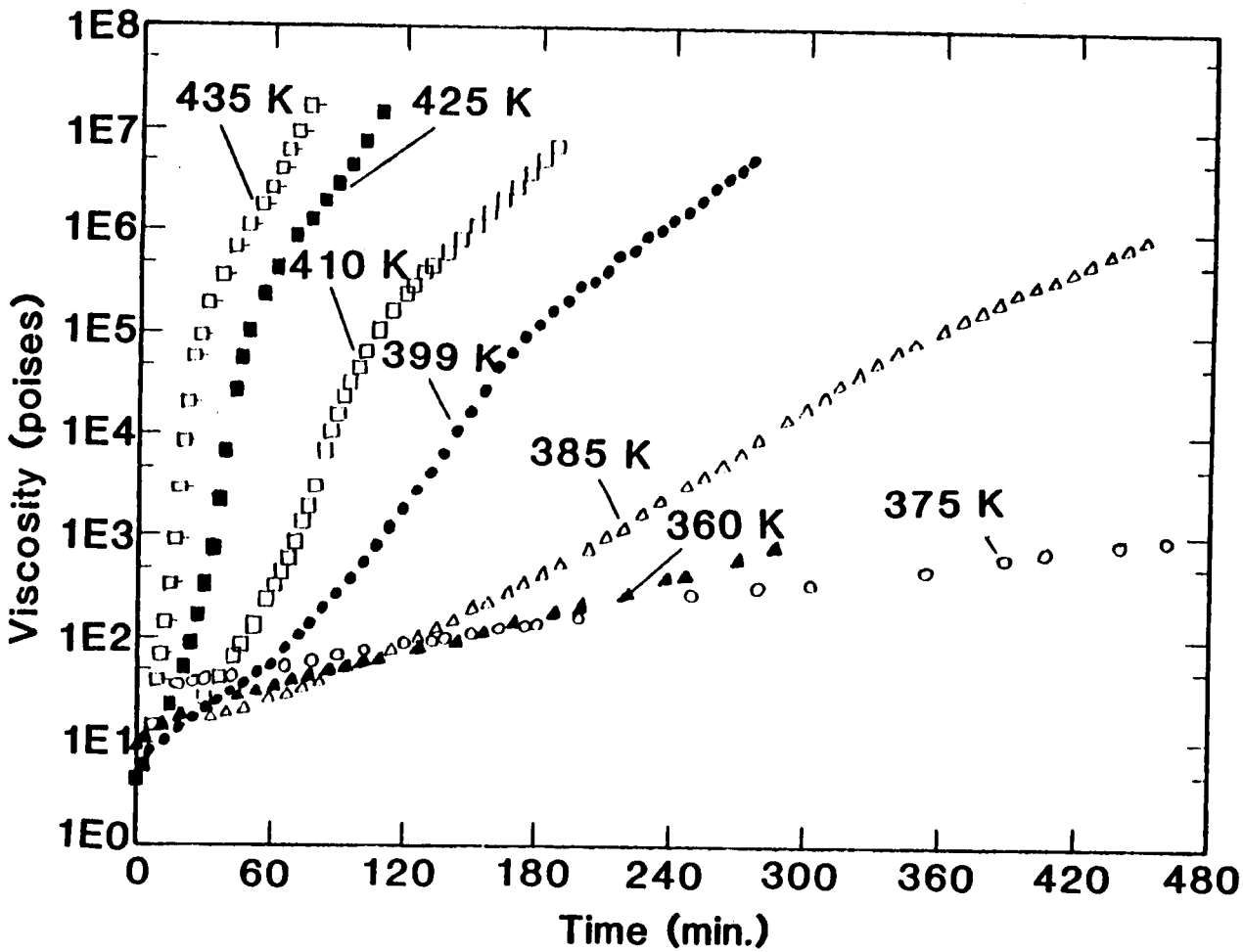

Fig. 4.8 Plot of chemoviscosity vs. time t for Hercules 3501-6 resin system under seven isothermal curing temperatures shown.

shorter curing time is needed for reaching the same viscosity level. For a given time, t, the initial decrease of viscosity during the curing was attributed to the temperature effects. Apparently, the non-linearity of the isothermal viscosity vs. time exists for the material.

4.3.2 Dynamic Case

Experimental results of chemoviscosity in the dynamic case are shown in Figs. 4.9-4.11. Three different dynamic heating rates of 2, 3 and 5 K/min were used. The initial decrease in viscosity is caused by the increase in curing temperature. At the gelation, the viscosity is noted to increase exponentially.

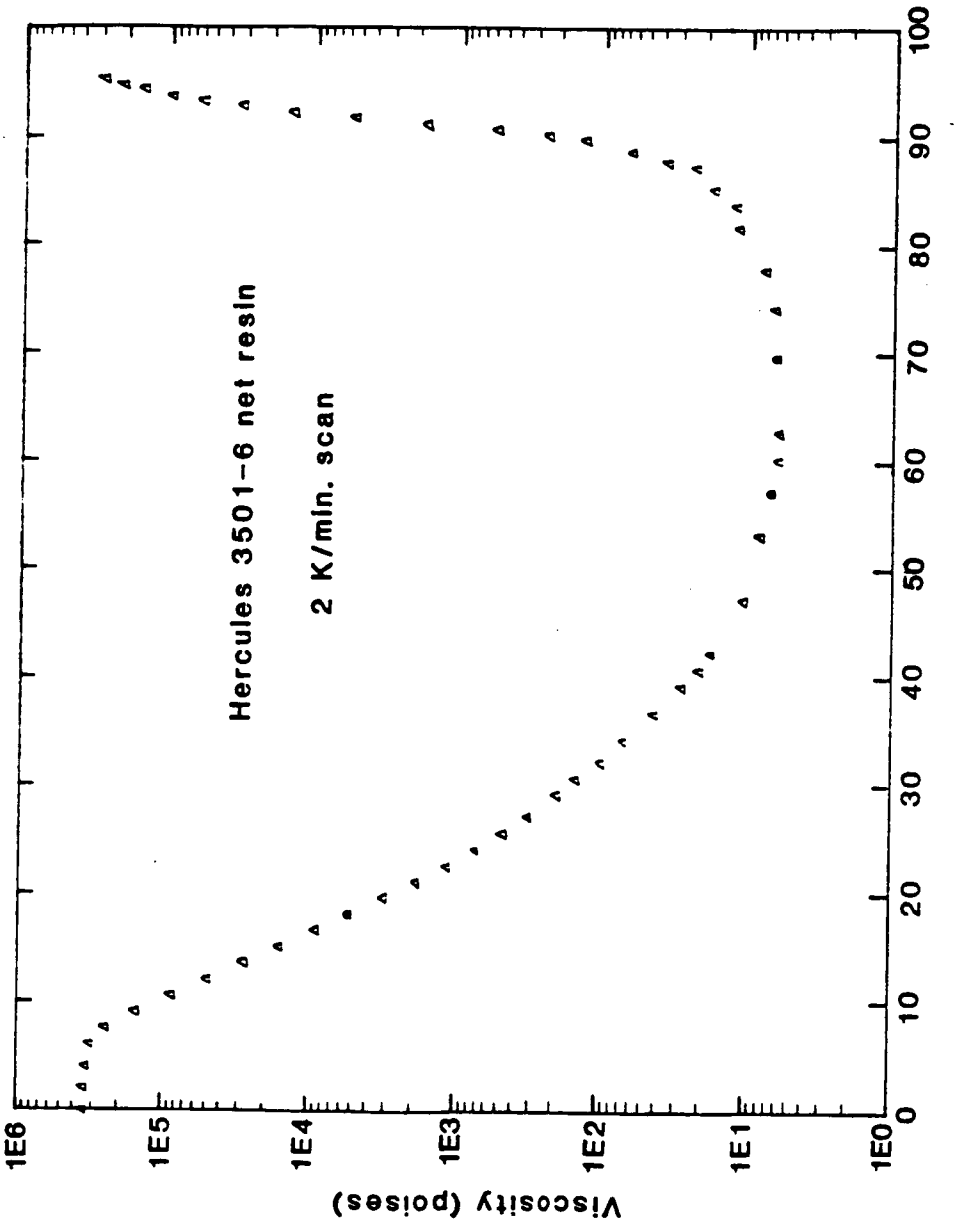

Fig. 4.9 Plot of chemoviscosity η vs. time t for Hercules 3501-6 resin system under dynamic curing condition at 2 K/min.

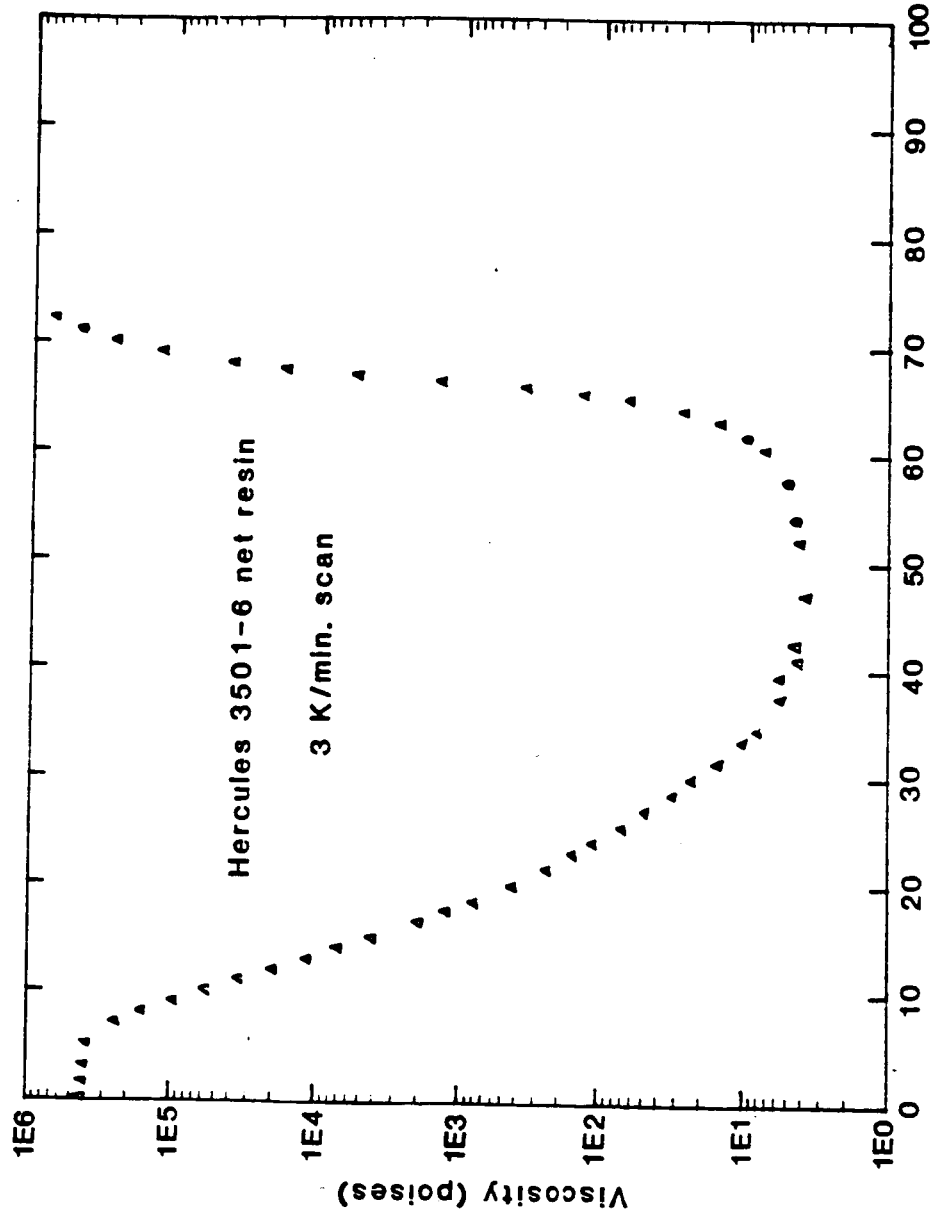

Fig. 4.10 Plot of chemoviscosity η vs. time t for Hercules 3501-6 resin system under dynamic curing condition at 3 K/min.

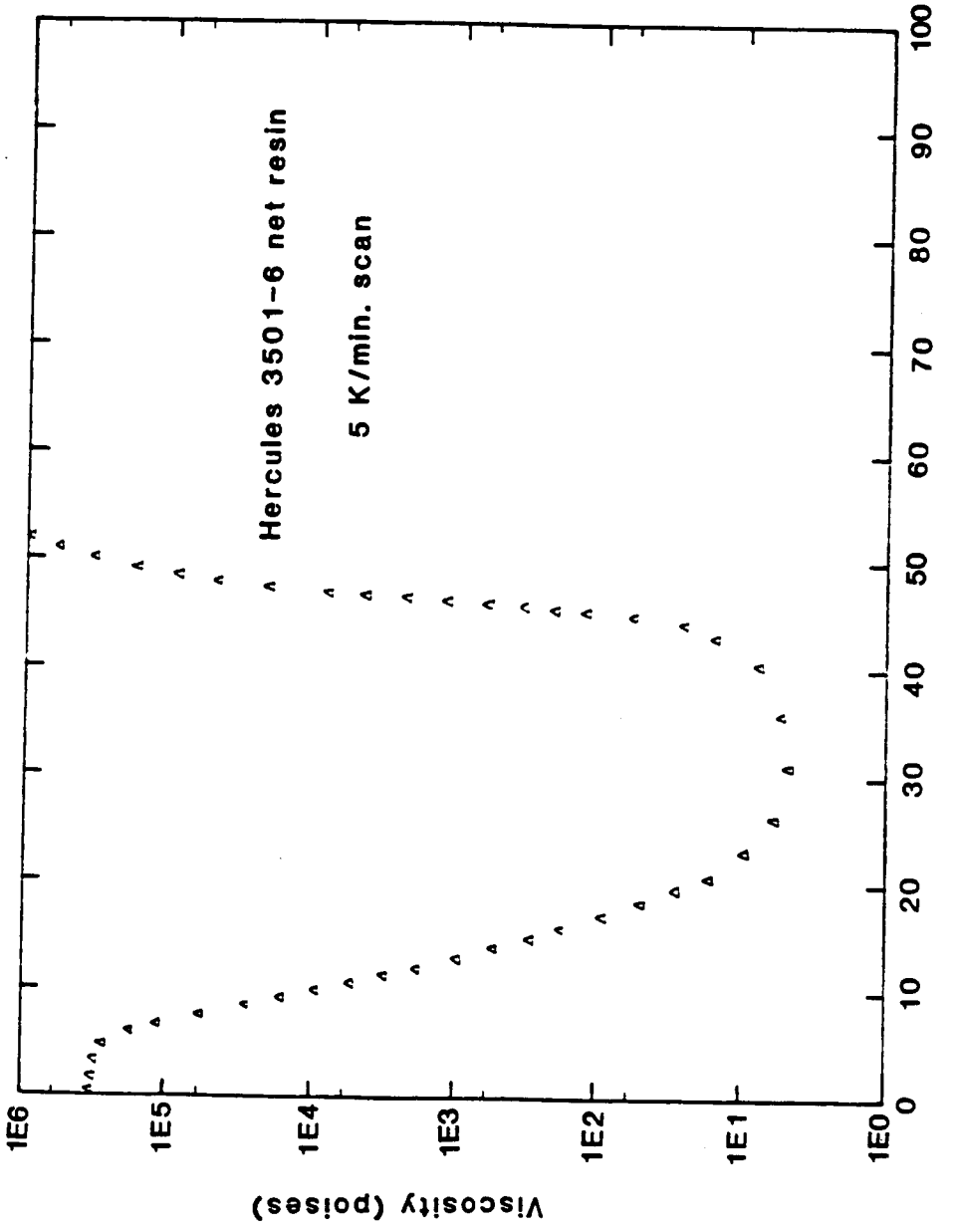

Fig. 4.11 Plot of chemoviscosity η vs. time t for Hercules 3501-6 resin system under dynamic curing condition at 5 K/min.

Chapter 5

CHEMOVISCOSITY MODELING

5.1 Theory

The Williams-Landel-Ferry (WLF) theory [6] states that for Tg < T < (Tg+100 K), the temperature-dependent viscosity is given by the expression

$$\log\left(\frac{\eta_T}{\eta_{Tg}}\right) = -\frac{C_1(T-Tg)}{C_2 + T-Tg} \tag{5.1}$$

where C_1 and C_2 are material constants. The temperature dependency of the viscosity as shown in Eq. (5.1) has been tested and found valid for materials ranging from dilute polymeric systems and thermoplastic melts to rubbers and elastomer. Equation (5.1) can be derived from the semi-empirical Doolittle equation which relates the viscosity to the free volume of the liquid. This will be discussed later in this chapter.

The normal use of the WLF equation for thermoplastic materials requires that the glass transition temperature Tg be constant while the temperature T is varied for the specific polymer under study. Equation (5.1) is applicable for a temperature T up to 100 K higher than the Tg of the material. However, during cure of thermosetting resin, the monomers are initially polymerized and crosslinks are formed later. This is a system where Tg(t) is changing and the curing temperature T is

held constant (e.g. the isothermal case). The glass transition temperature Tg rises continuously and eventually approaches the curing temperature. Over the entire curing cycle, the material structure actually undergoes a continuous phase transformation from the low molecular weight liquid to the high molecular weight polymeric melt, and eventually transforms to form crosslinking networks. If it is assumed that Tg(t) of the material is always lower than the cure temperature T, and that (T-Tg(t)) is always within 100 K, then the WLF theory should be applicable to all polymer structure phases during the cure. However, before Eq. (5.1) can be applied to describe the chemoviscosity of the curing resin, modifications have to be made to properly account for the reaction time, t, of the thermosetting resin system.

One method of introducing reaction time factor into the WLF equation is to express the glass transition temperature Tg(t) as a function of $\alpha(t)$, the degree of cure. Several different techniques have been used in literature which include thermal, spectrophotometric (FTIR) and chromatographic (HPLC) measurements to determine the extent of cure. In the present study, we assume that for the resin system under investigation, $\alpha(t)$ at time t is equal to the fraction of heat released, as measured by DSC, up to time t for the resin system under cure. The α's thus determined are a function of the curing temperature and time. The two material constants, C_1 and C_2, should be varied with reaction time because of the transformation of different material structures during cure.

5.2 Chemoviscosity Modeling

The procedure used in modeling of chemoviscosities of Hercules 3501-6 epoxy resin is described by the following two steps:

1. Temperature-dependent material constants $C_1(T)$ and $C_2(T)$ in Eq. (5.1) are first determined by the experimental data for the material cured under isothermal condition.
2. The chemoviscosity $\eta(t,T)$ established by isothermal cure data under procedure 1 is allowed to follow various dynamic heating cure cycles $T(t)$. The viscosity values thus calculated are compared with the experimental data.

5.2.1 Isothermal Case

For the material cured isothermally, the relationship between degree of cure $\alpha(t)$ and curing time t is established by integrating the kinetics model of Lee et al. [5]. As discussed in Chap. 4, this is given by

$$t = \frac{a}{K_{n_2}} \ln\left(1 + \frac{K_{n_2}}{K_{n_1}} \alpha\right) - b \ln (1-\alpha) - c \ln \left(1 - \frac{\alpha}{B}\right) \quad \alpha < 0.3 \qquad (4.4a)$$

$$t = -\frac{1}{K_{n_3}} \ln \left(\frac{1-\alpha}{0.7}\right) + tc \quad \alpha > 0.3 \qquad (4.4b)$$

The glass transition temperature $Tg(t)$ and the degree of cure $\alpha(t)$ is related experimentally by

$$Tg = d1(T)\ \alpha(t) + d2 \qquad (4.5)$$

where

$$\text{Logd1}(T) = -639.56/T + 3.357 \qquad T < 450\ K \qquad (4.6a)$$

$$\text{Logd1}(T) = -3216.49/T + 8.879 \qquad T > 450\ K \qquad (4.6b)$$

$$d2 = 283.0$$

Substituting Eqs. (4.4a), (4.4b) and (4.5) into Eq. (5.1), the calculated $\alpha(t)$ at a given isothermal cure condition can be made to fit the experimental data through the adjustments of the two material constants C_1 and C_2. During the model calculation, η_{Tg} is assigned a value of 10^{13} poises. This is the viscosity determined at Tg for many glass-forming substances and polymer systems [16].

The $C_1(T)$ and $C_2(T)$ values determined for seven different temperatures are listed in Table 5.1, and the model predictions are drawn as a solid line in Figs. 5.1 to Fig. 5.7. It is noted that the model is capable of describing the non-linear relationship between viscosity which is below the order of 10^3. This is considered a significant improvement over the empirical linear model used by Lee et al. [5].

An Arrhenius plot of C_1 and C_2 respectively, vs. temperature, is shown in Figs. (5.8) and (5.9). The linear Least Square technique was used again and was found to fit the data reasonably well. The two straight lines are represented, respectively, by

$$C1 = 4.067 \times 10^4 \frac{1}{T} - 54.252 \qquad \text{for } T < 382\ K \qquad (5.2a)$$

Table 5.1 Values of C_1 and C_2 determine for seven different temperatures under isothermal condition.

Tc (K)	C_1	C_2
360	59.0	300
375	53.5	300
385	51.8	300
399	85.7	600
410	110.7	850
425	128.7	1100
435	133.4	1300

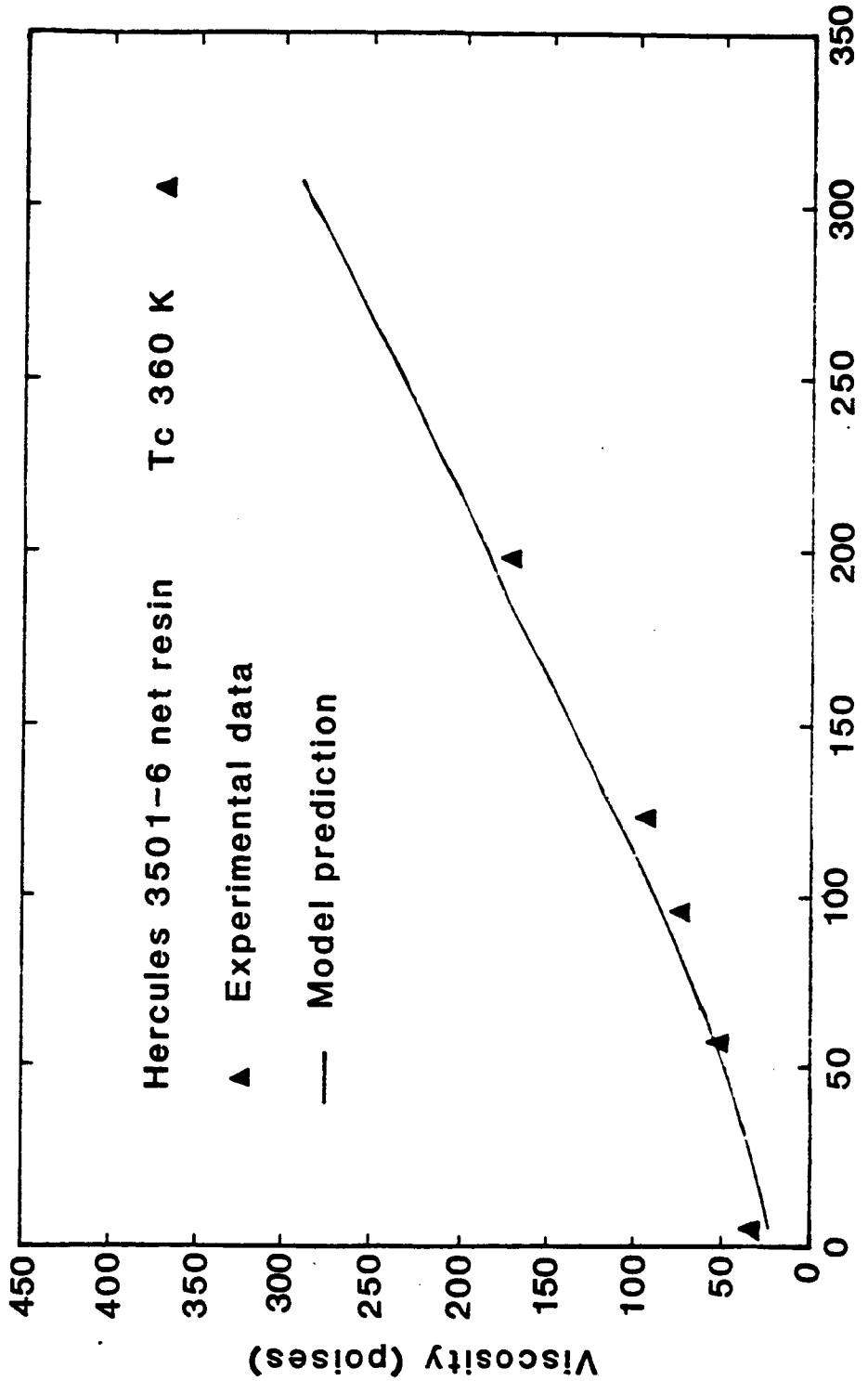

Fig. 5.1 Chemoviscosity of Hercules 3501-6 resin system cured under isothermal curing temperature 360 K; triangles denote the experimental data; solid curve denotes the model prediction of Eq. (5.1).

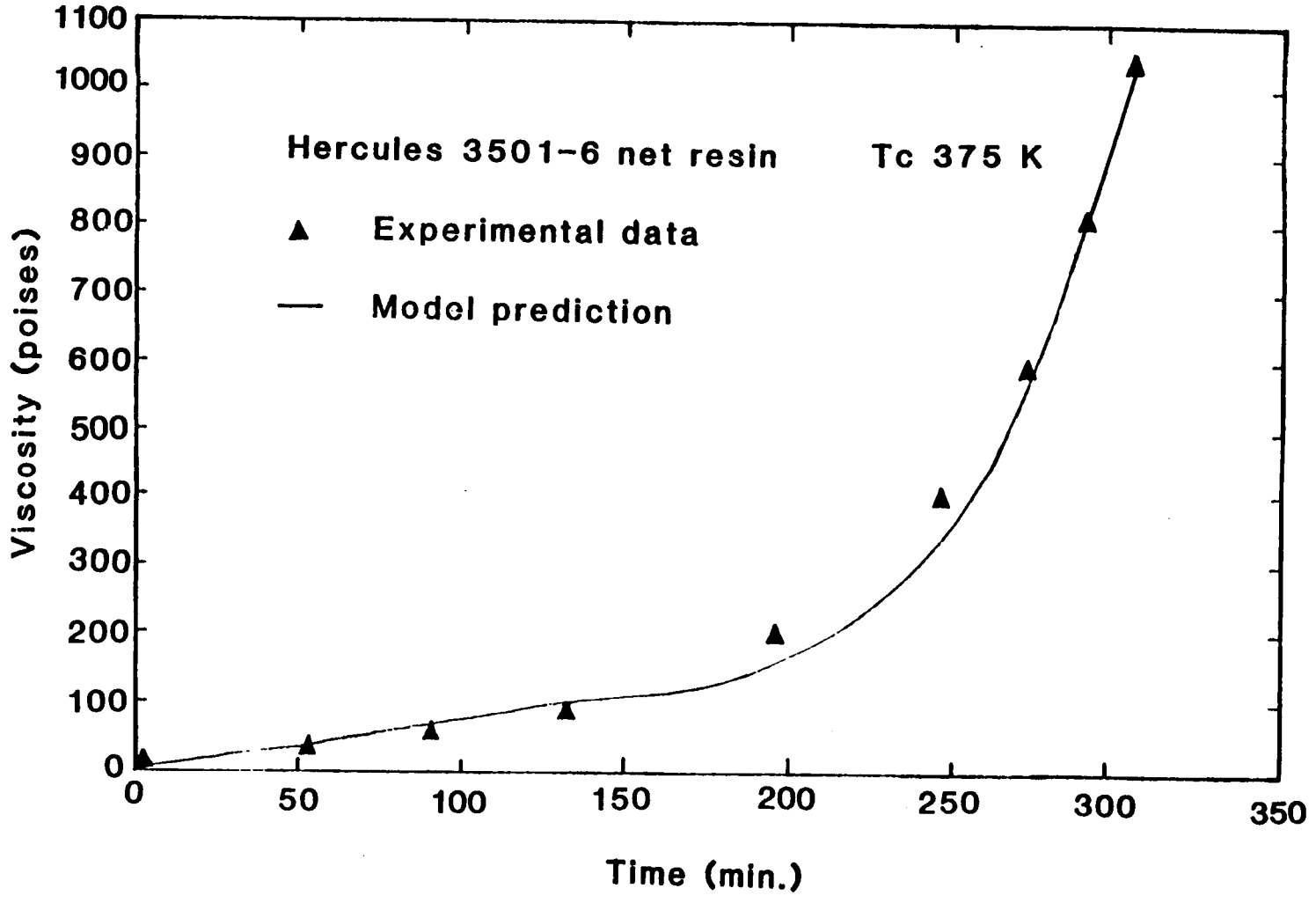

Fig. 5.2 Chemoviscosity of Hercules 3501-6 resin system cured under isothermal curing temperature 375 K; triangles denote the experimental data; solid curve denotes the model predictions.

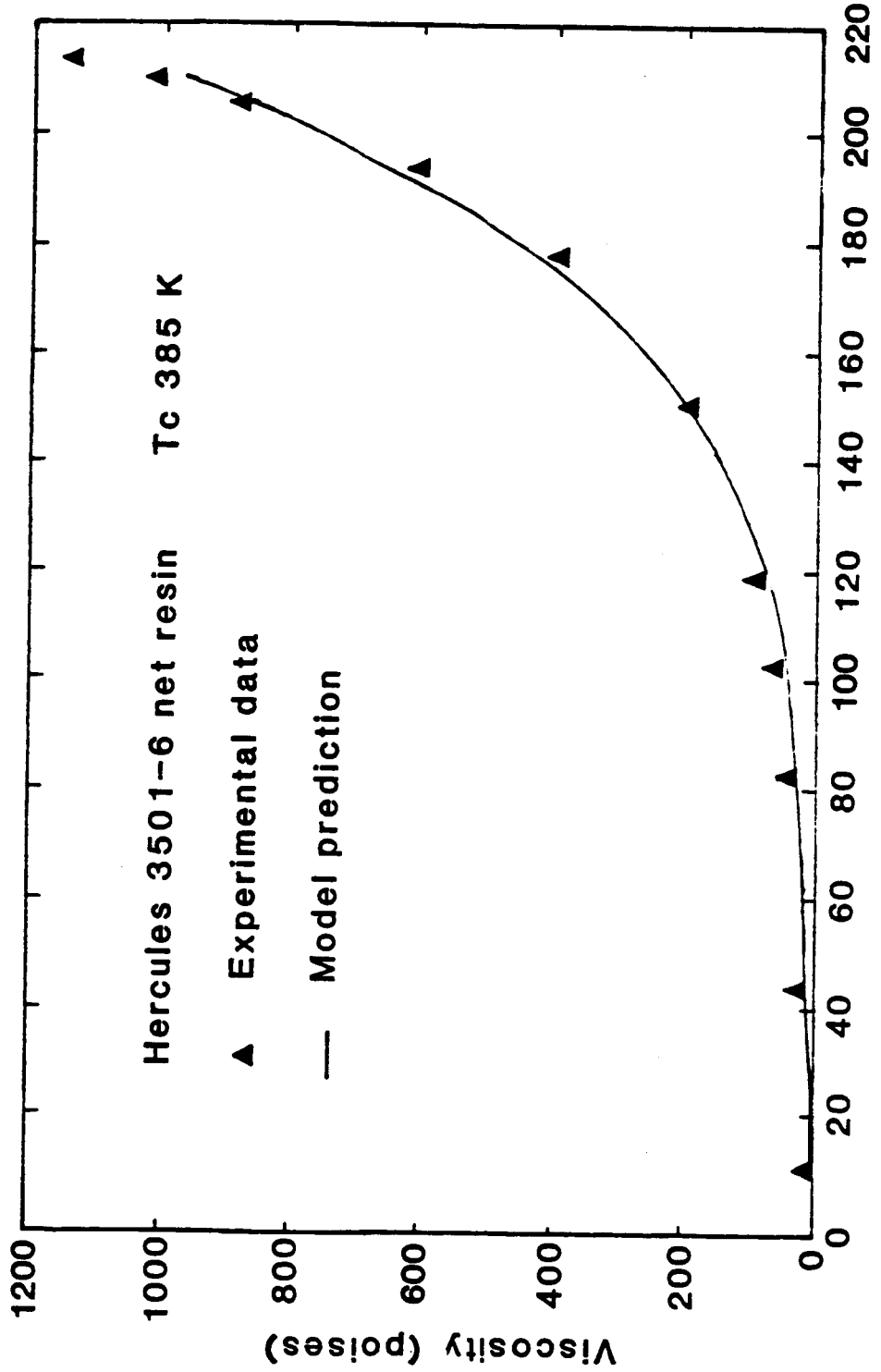

Fig. 5.3 Chemoviscosity of Hercules 3501-6 resin system cured under isothermal curing temperature 385 K; triangles denote the experimental data; solid curve denotes the model prediction of Eq. (5.1.).

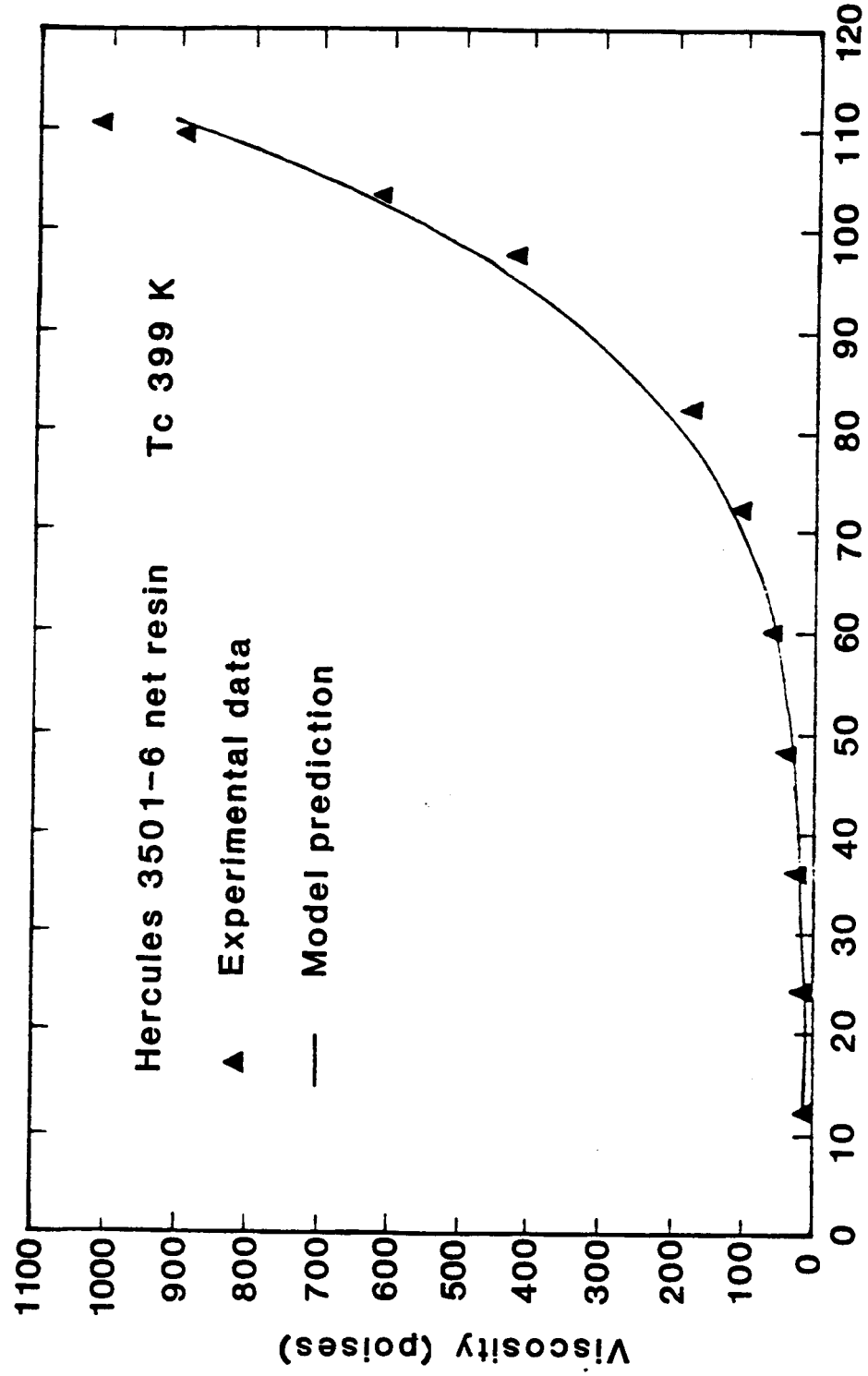

Fig. 5.4 Chemoviscosity of Hercules 3501-6 resin system cured under isothermal curing temperature 399 K; triangles denote the experimental data; solid curve denotes the model prediction of Eq. (5.1).

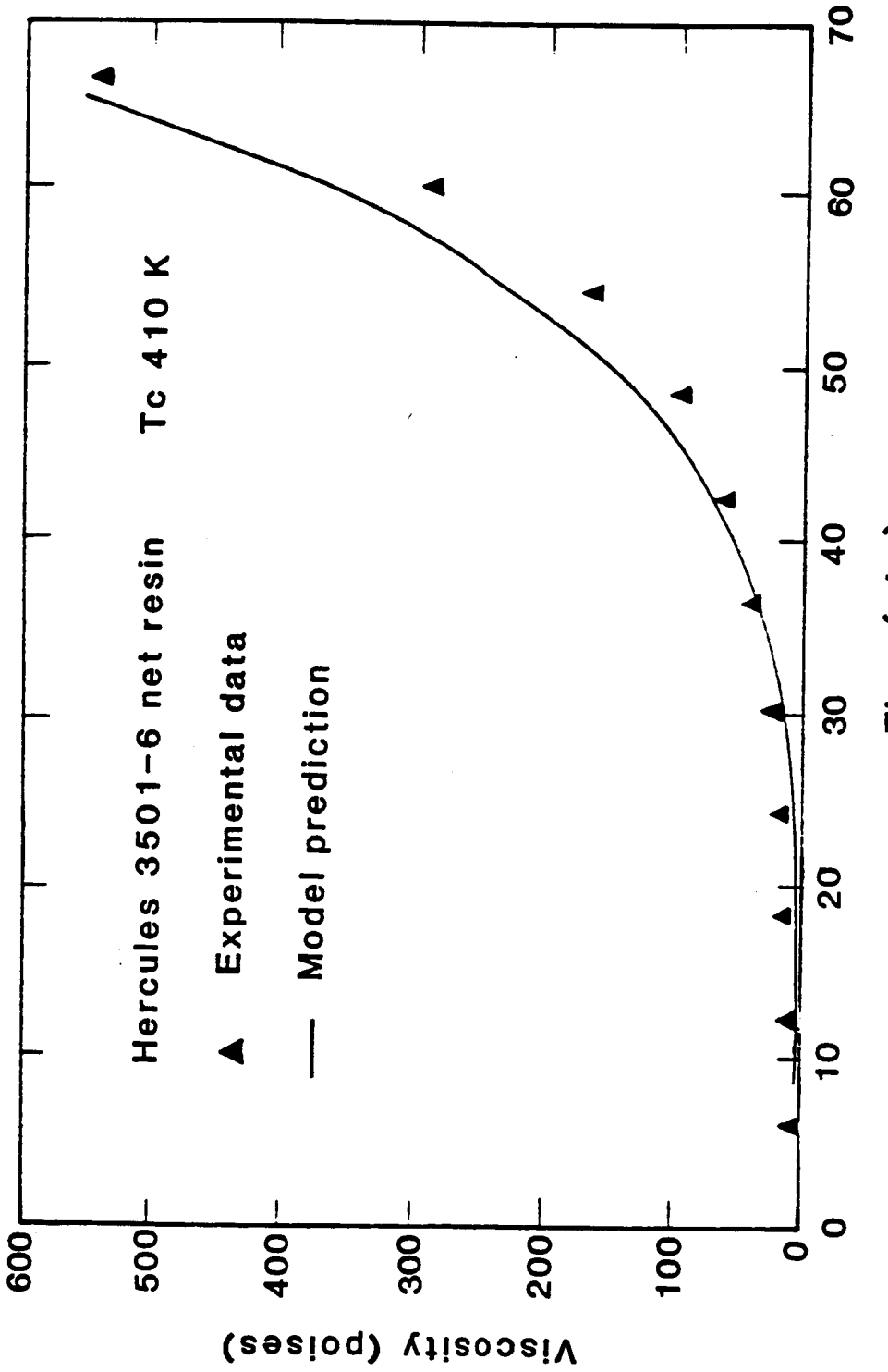

Fig. 5.5 Chemoviscosity of Hercules 3501-6 resin system cured under isothermal curing temperature 410 K; triangles denote the experimental data; solid curve denotes the model prediction of Eq. (5.1).

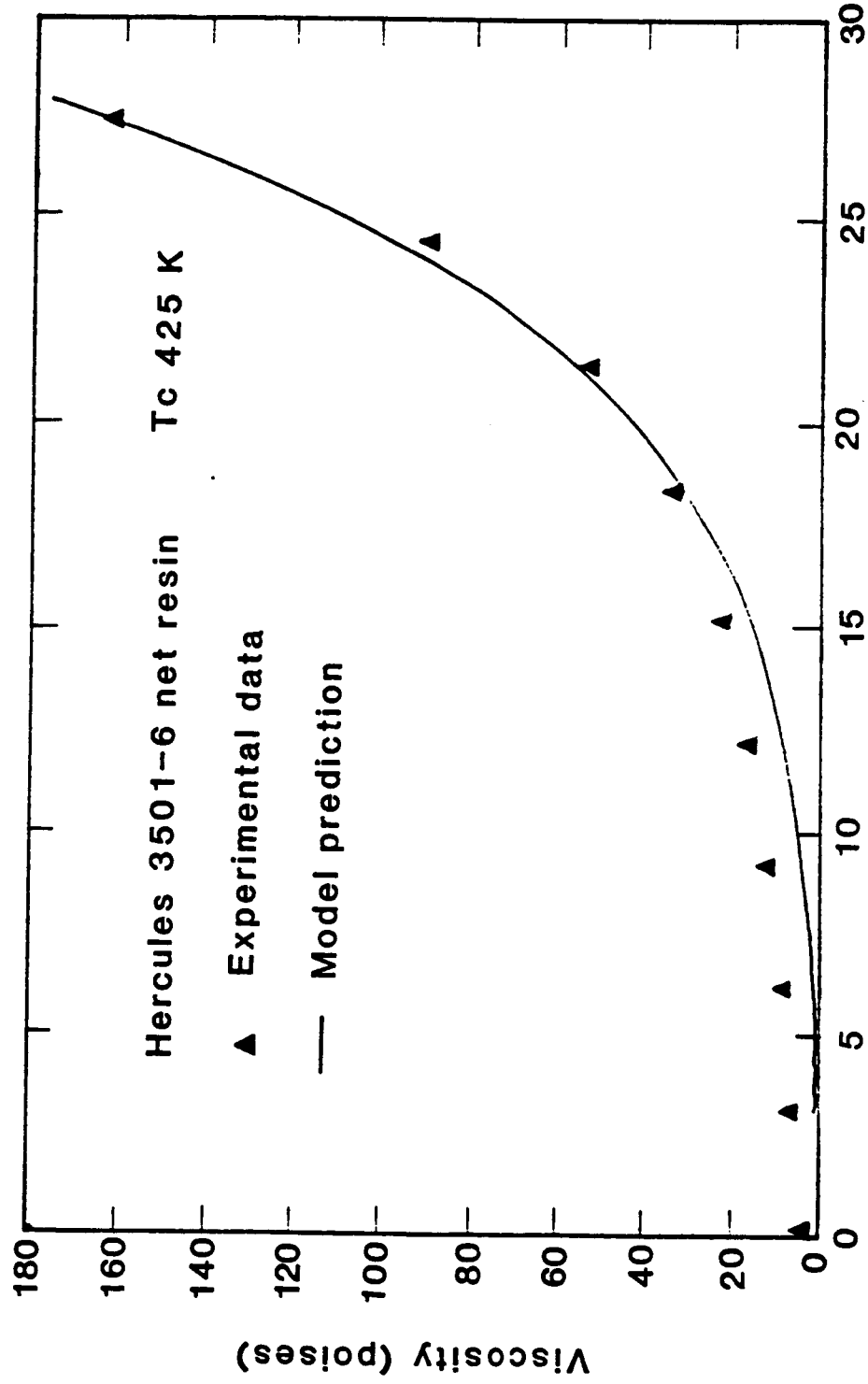

Fig. 5.6 Chemoviscosity of Hercules 3501-6 resin system cured under isothermal curing temperature 425 K; triangles denote the experimental data; solid curve denotes the model prediction of Eq. (5.1).

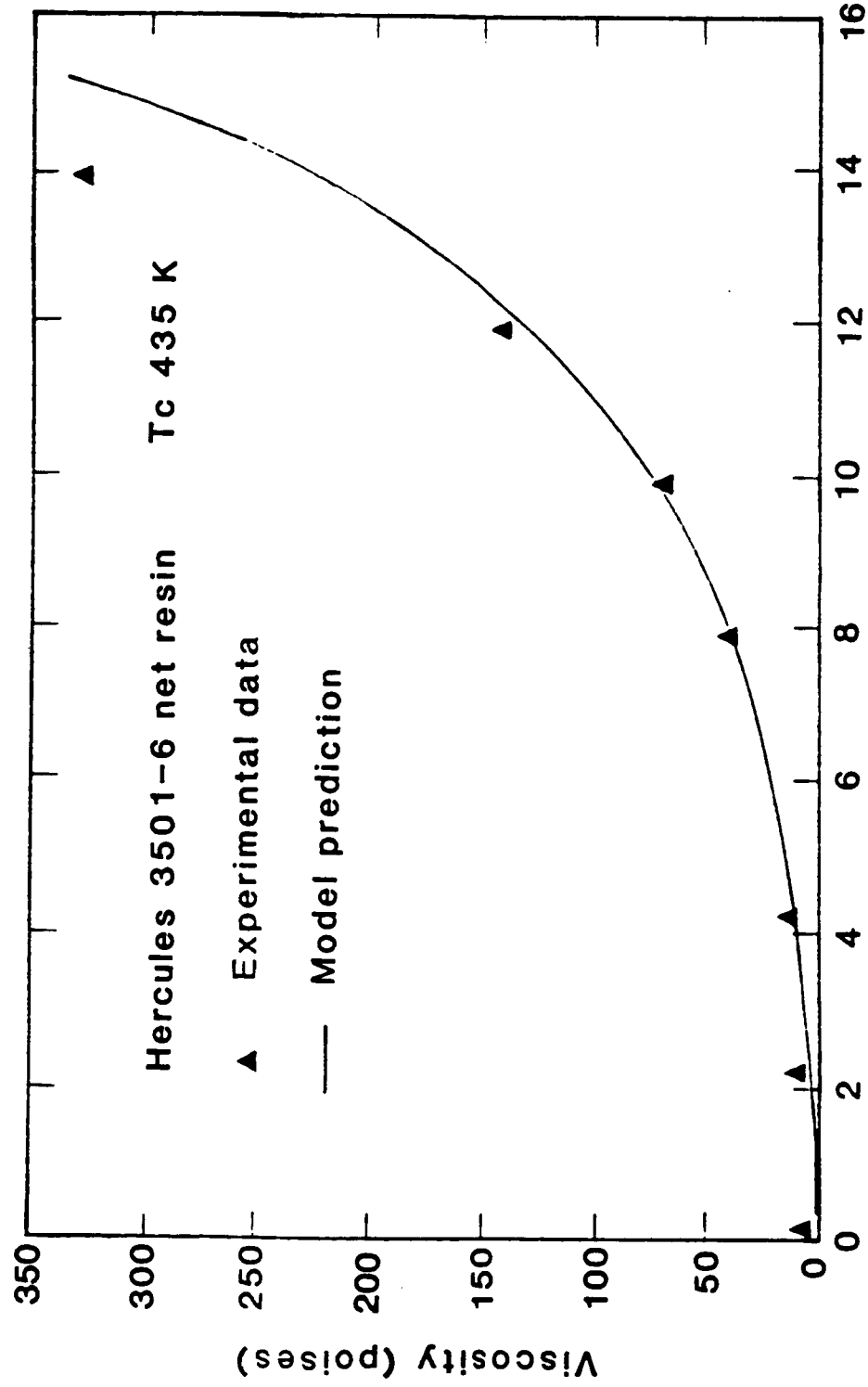

Fig. 5.7 Chemoviscosity of Hercules 3501-6 resin system cured under isothermal curing temperature 435 K; triangles denote the experimental data; solid curve denotes the model prediction of Eq. (5.1).

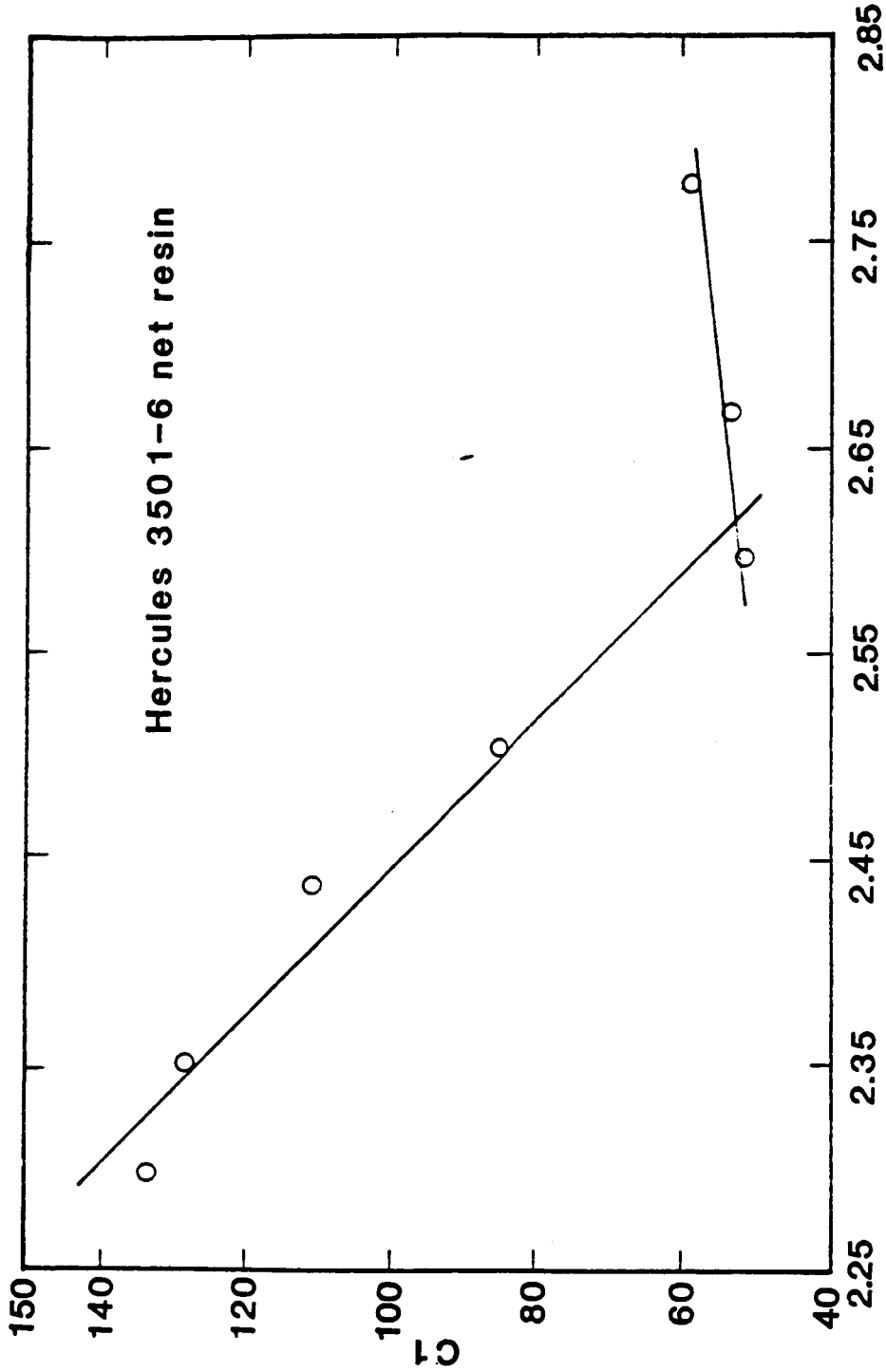

Fig. 5.8 Plot C1(T) of Eq. (5.1) vs. 1/T for Hercules 3501-6 resin system.

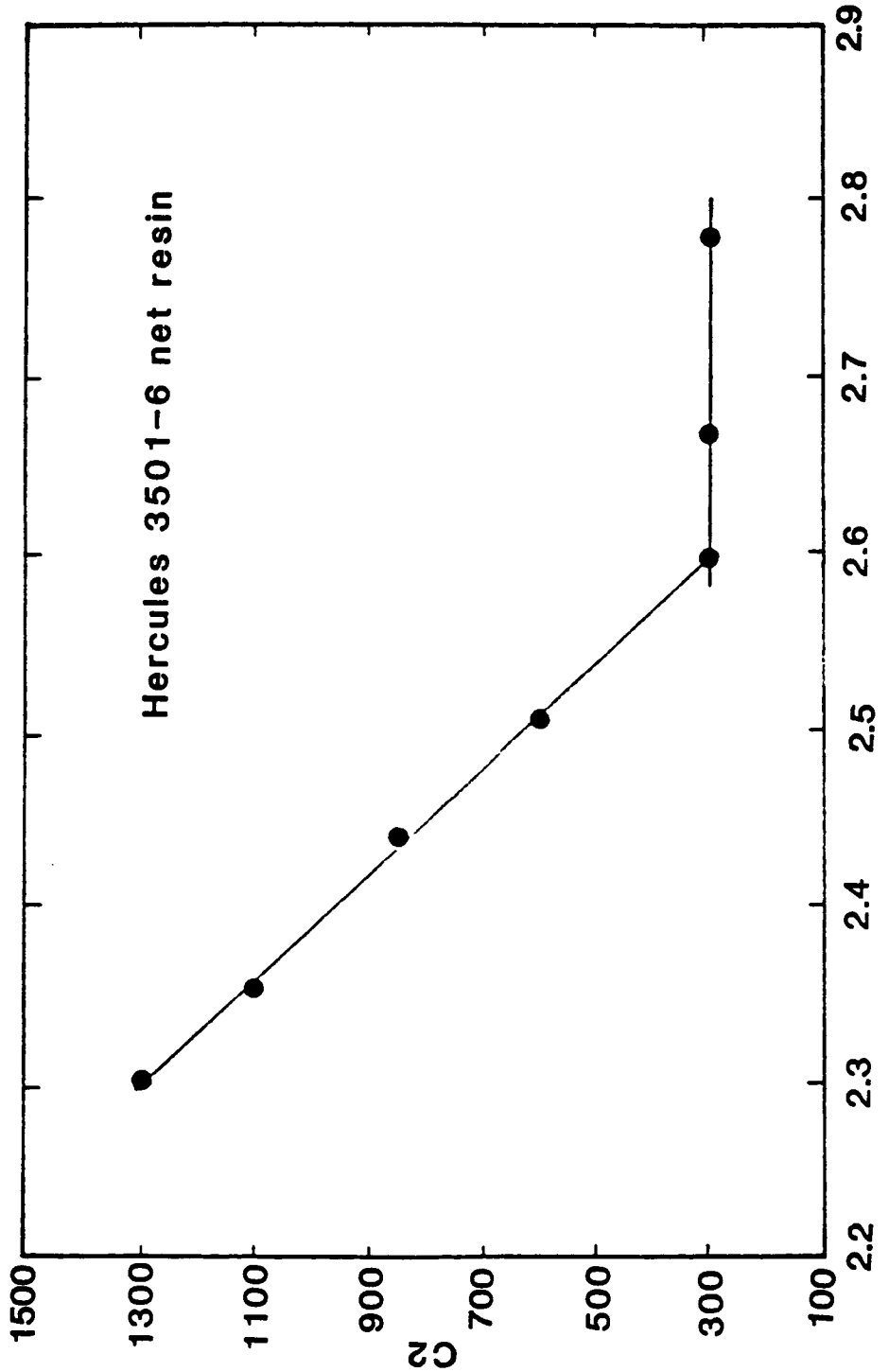

Fig. 5.9 Plot of C2(T) of Eq. (5.1) vs. 1/T for Hercules 3501-6 resin system.

$$C2 = 300$$

$$C1 = 1\ 2.776\times10^{5}\ \frac{1}{T}\ 779.09 \qquad \text{for } T > 382\ K \qquad (5.2b)$$

$$C2 = -3.33\times10^{6}\ \frac{1}{T} + 8959.65$$

These temperature dependent $C_1(T)$ and $C_2(T)$ are used to simulate the chemoviscosity-time profiles under dynamic heating cases.

5.2.2 Dynamic Heating Case

Similar techniques as those used in the isothermal cases are employed here. The advancement in the degree of cure under dynamic heating conditions can be calculated from Eqs. (4.1a) and (4.1b) by means of the Taylor's series expansion as discussed in Sec. 4.2. By substituting Eqs. (4.5), (5.2a) and (5.2b) into Eq. (5.1), the chemoviscosity-time profiles for the resin system cured under dynamic heating conditions can be simulated.

Values of $\alpha(t)$ determined by the Taylor's series expansion depend slightly on the time interval Δt chosen. Theoretically, $\alpha(t)$ can be determined more accurately when a smaller Δt is used. The effect of step size Δt on the calculated degree of cure $\alpha(t)$ is given in Table 5.2. The differences in $\alpha(t)$ are within 2% and are negligible. The step size of $\Delta t=0.01$ was chosen for all calculations.

Chemoviscosities of the Hercules 3501-6 epoxy resin system under dynamic heating cure condition were obtained at heating rates 2, 3 and 5 K/min, respectively. All cure cycle were started at 300 K. The results of the model predictions are shown as solid curves in Figs. 5.10-5.11.

Table 5.2 The calculated degree of cure $\alpha(t)$ by different time step size Δt

Curing Time (min)	$\alpha(t)$		
	$\Delta t=0.01$	$\Delta t=0.05$	$\Delta t=0.1$
6	.150226	.153258	.157127
8	.347579	.351781	.357062
10	.606030	.611808	.619061
12	.899822	.904560	.910432

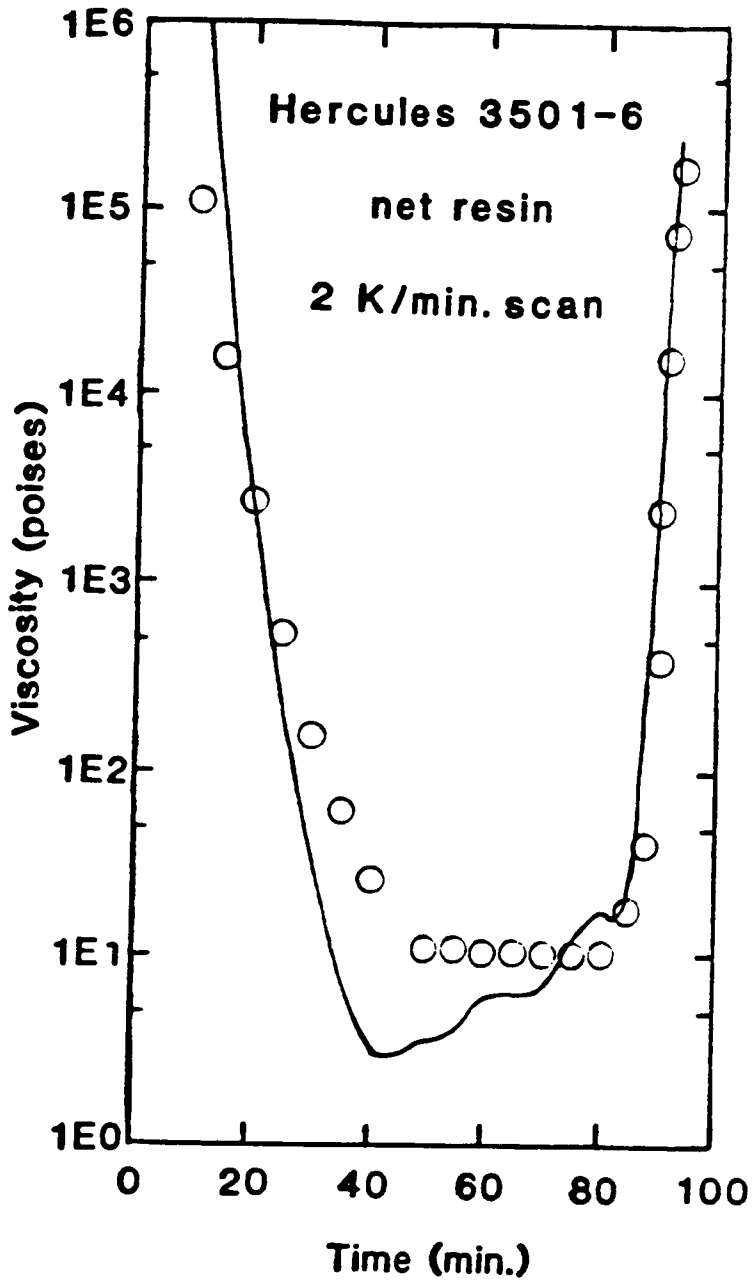

Fig. 5.10 Chemoviscosity of Hercules 3501-6 resin system under dynamic curing condition at heating rate of 2 K/min; circles denote the experimental data; solid curve denotes the model prediction of Eq. (5.1).

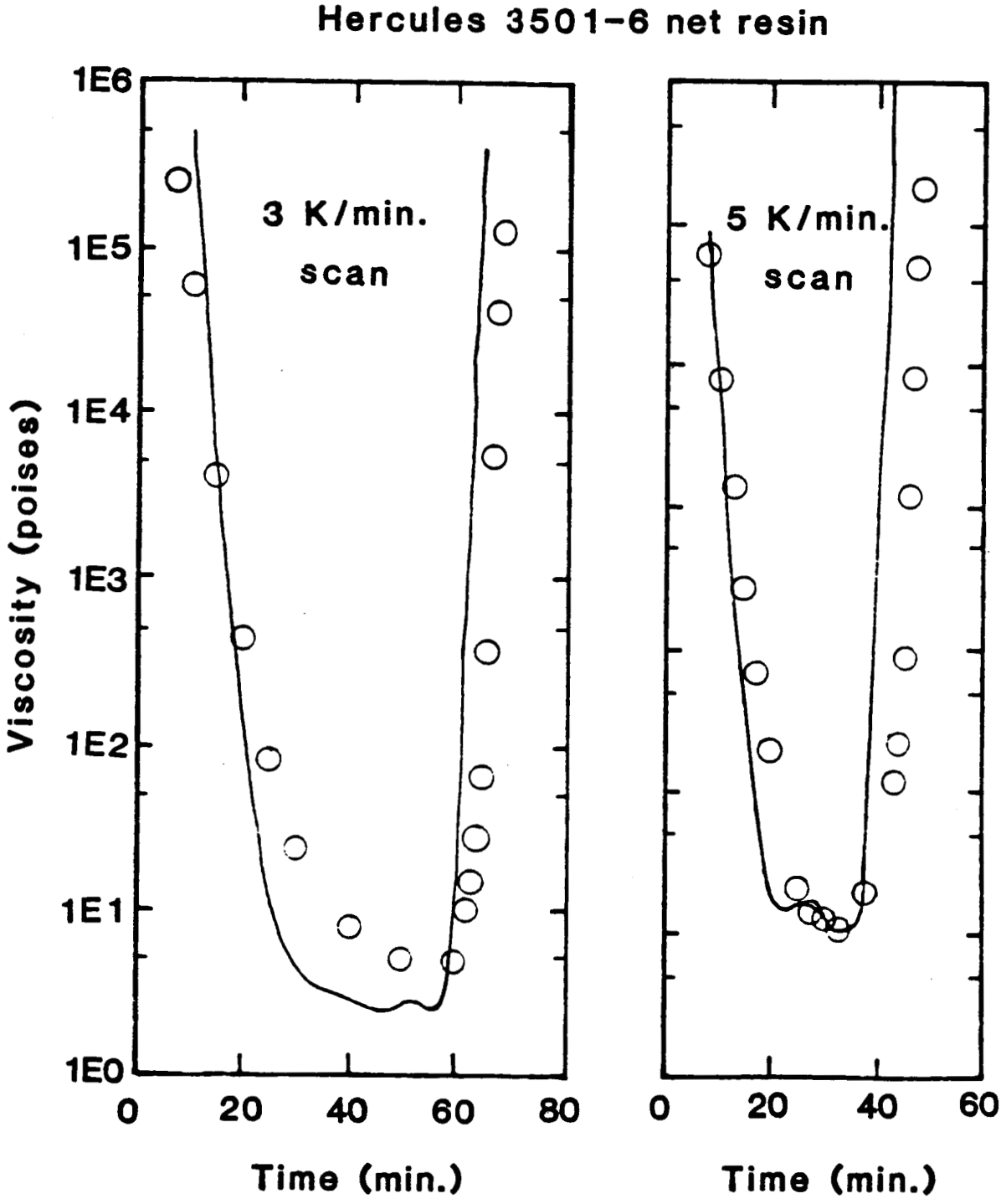

Fig. 5.11 Chemoviscosity of Hercules 3501-6 resin system under dynamic heating condition at heating rate of 3 and 5 K/min. respectively; circles denote the experimental data; solid curves denote the model prediction of Eq. (5.1).

It is noted that the model calculations compared favorably with the experimental data for all three cases.

The WLF model used in the present study was originally derived from the semiempirical Doolittle equation for the viscosity of a liquid as [17]

$$\ell n\eta = \ell nA'' + B'' \left(\frac{V - V_f}{V_f}\right) \tag{5.3}$$

This gives an expression for the viscosity of a system in terms of two constants A and B. The quantity V is the total volume of the system while V_f is the free volume available to the system. Rearrangement of Eq. (5.3) gives

$$\ell n\eta = \ell nA'' + B'' \left(\frac{1}{f} - 1\right) \tag{5.4}$$

where f is the fractional free volume V_f/V. It is assumed that above the glass transition temperature, the fraction free volume increases linearly, that is

$$f = fg + \alpha_f (T - Tg) \qquad T > Tg \tag{5.5}$$

where f is the fractional free volume at T, fg is the fractional free volume at Tg, and α_f is the thermal coefficient of expansion of the fractional free volume above Tg. Substituting Eq. (5.5) into (5.3), the Doolittle equation becomes

$$\text{Log } \frac{\eta_T}{\eta_{Tg}} = - \frac{B''}{2.303\ fg} \left(\frac{T-Tg}{\left(\frac{fg}{\alpha_f}\right) + T-Tg}\right) \tag{5.6}$$

Equations (5.1) and (5.6) have the same form, and we can have

$$C1 = \frac{B''}{2.303\ f_g}$$
$$C_2 = \frac{f_g}{\alpha_f} \qquad (5.7)$$

where B'', a parameter in the Dolittle equation, is experimentally found to be close to unity.

The concept of free volume is difficult to derive in a precise manner. In an approximate way, we can represent the segment of a polymer chain by rigid bodies and the free volume as the holes presented between these segments as a result of packing requirements. Presumably, the free volume reaches a constant value at Tg, which is too small to allow the large-scale conformational rearrangements of the chain backbones associated with Tg to occur. Above Tg, on the other hand, free volume increases and becomes sufficiently large to allow such motions to occur.

The constants C_1 and C_2 have been shown to vary from polymer to polymer [18]. During the curing of thermosetting resin, the mononers are initially polymerized and crosslinks are formed later. The material undergoes continuous phase changes from dilute polymeric solutions to polymer melts, and eventually the elastomers. A single set of C_1 and C_2 for each isothermal curing condition is found here, however, to describe the chemoviscosity-time profile adequately. This single set of values is therefore considered to describe a material state which represents an average over various structures occurring inside the material during cure. Values of C_1 and C_2 do vary with different isothermal curing temperatures as can be seen in Table 5.1. The fractional free volume and thermal expansion coefficient calculated by Eq. (5.7) are given in Table 5.3.

Table 5.3 The values of the fractional free volume and thermal expansion coefficient determined under isothermal condition

Curing Temperature Tc (K)	C1	C2	fg	α_f(1/K)
360	59.0	300	7.36E-3	2.45E-5
375	53.5	300	8.12E-3	2.71E-5
385	51.8	300	8.38E-3	2.79E-5
399	85.7	600	5.07E-3	8.45E-6
410	110.7	850	3.83E-3	4.61E-6
425	128.7	1100	3.37E-3	3.06E-6
435	133.4	1300	3.26E-3	2.51E-6

For the thermosetting resin system studied here, the magnitude of fractional free volume is determined by two competing factors. On one hand, higher curing temperatures create larger dilatational effects, which then generate larger free volume inside the material; on the other hand, increasing molecular weights as a result of polymerization reactions reduce the free volume due to the eliminations of number of molecular chain ends. The initial decrease in the fractional free volume fg from Tc = 360 to 385 K is, therefore, attributed to the increasing dilatation effects at higher curing temperatures. This is also consistent with the slower advancement of reactions observed in the chemoviscosity-time profiles in this temperature range. The decrease in fg from Tc = 385 to 435 K suggest that at this temperature range, the polymerization reaction becomes a dominant factor.

Chapter 6

CONCLUSIONS AND RECOMMENDATIONS

A new analytical model for simulating chemoviscosity of thermosetting resin has been formulated. The model is developed by modifying the well-established Williams-Landel-Ferry (WLF) theory in polymer rheology for thermoplastic materials. From this investigation, the following conclusions and recommendation are provided:

1. By introducing relations between the glass transition temperature $Tg(t)$ and the degree of cure $\alpha(t)$ of the resin system under cure, the WLF theory is modified to account for the factor of reaction time. Thus the model proposed is capable of simulating viscosity profiles in various cure cycles.

2. The reaction kinetics established based on the isothermal cure condition on the resin system is related to the case of dynamic curing condition. This also provides the relation for the viscosity in the isothermal and dynamic cases.

3. The glass transition temperature $Tg(t)$ in the isothermal case is dependent not only on the reaction time t, but also on the cure temperature T. Nevertheless, the relationship of glass transition temperature $Tg(t)$ and degree of cure $\alpha(t)$ established is also valid for the case of dynamic curing condition.

4. A single set of C_1 and C_2 is found to describe adequately a material state which represents an average over various structures that occur inside during each isothermal curing condition. Thus, the $C_1(T)$ and $C_2(T)$ may be included in the model to predict the chemoviscosity profiles under dynamic curing conditions. Theoretical results obtained from this model compare favorably well with the experimental data.

5. It is recommended that the present research be extended to explore the application of the model to large scale processing.

REFERENCES

1. Tajima, Y. A. and Crozier, D., "Thermokinetic Modeling of an Epoxy Resin-I Chemoviscosity," Polymer Engineering Science, Vol. 23, April 1983, pp. 186-190.

2. Kay, A. O. and Maddock, B. C., "Exploratory Development on Processing Science of Thick-Section Composites," Lockheed-Georgia Co., Atlanta, Georgia, F33615-82-C-5059, Jan. 1984.

3. Roller, M. B., "Characterization of the Time-Temperature-Viscosity Behavior of Curing B-Stage Epoxy Resin," Polymer Engineering Science, Vol. 15, June 1975, pp. 406-414.

4. Carpenter, J. F., "Processing Science for AS/3501-6 Carbon/Epoxy Composites," McDonnell Aircraft Co., St. Louis, MO, N00019-81-C-0184, Jan. 1982.

5. Lee, W. I., Loos, A. C. and Springer, G. S., "Heat of Reaction Degree of Cure and Viscosity of Hercules 3501-6 Resin," Journal of Composite Materials, Vol. 16, 1982, pp. 510-520.

6. Williams, M. L., Landel, R. F. and Ferry, J. D., "The Temperature Dependence of Relaxation Mechanisms in Amorphous Polymers and Other Glass-Forming Liquids," Journal of the American Chemistry Society, Vol. 77, July 1955, pp. 3701-3707.

7. Tajima, Y. A. and Crozier, D., "Chemorheology of an Amine Cured Epoxy Resin," SPE ANTEC Conference Proceedings, Society of Plastics Engineers, Vol. 30, May 1984, pp. 274-277.

8. Apicella, A., Nicolais, L. and Halpin, J. C., "The Role of the Processing Chemo-Rheology on the Aging Behavior of High Performance Epoxy Matrices," 28th National SAMPE Symposium, Society of the Advancements of Material and Process Engineering, Vol. 28, 1983, pp. 518-527.

9. Hou, T. H., "Chemoviscosity Modeling for Thermosetting Resins-I," NASA-Langley Research Center, Hampton, Virginia, CR-172443, Nov. 1984.

10. "Instructions of Model DSC-2 Differential Scanning Calorimeter," Perkin-Elmer Corp., Norwark, CT, 1979.

11. Greenspan, D., Introduction to Numerical Analysis and Applications, Markham Publishing Co., Chicago, 1971.

12. Operations Manual of Rheometric System Four, Rheometrics Inc., Springfield, New Jersey, 1981.

13. Hou, T. H, Bai, J. M. and Tiwari, S. N., "Chemoviscosity Modeling for Thermosetting Resins-III, Chemorheology of Hercules 3501-6 Resin System," NASA Contractor Report (to appear).

14. Sewell, T. A., "Chemical Composition and Processing Specifications for Air Force/Navy Advanced Composite Matrix Materials," McDonnell Aircraft Co., St. Louis, MO, F33615-78-C-5177, Dec. 1982.

15. Conte, S. D., Elementary Numerical Analysis, McGraw-Hill Book Co., New York, 1965.

16. Gordon, M. and Simpson, W., "The Rate of Cure of Network Polymers and the Superposition Principle," Polymer, Vol. 2, April 1961, pp. 383-391.

17. Doolittle, A. K. and Doolittle, D. B., "Studies in Newtonian Flow V. Further Vertification of the Free-Space Viscosity Equation," Journal of Applied Physics. Vol. 28, Aug. 1957, pp. 901-905.

18. Aklnois, J. J., Macknight, W. J. and Shen, M., Introduction to Polymer Viscoelasticity, John Wiley & Sons, Inc., New York, 1972.

APPENDICES

APPENDIX A

EVALUATION OF TOTAL HEAT OF REACTION AND DEGREE OF CURE

The numerical analysis technique applied to determine the total heat of reaction and degree of cure is summarized in this appendix.

A thermogram obtained from the DSC under the dynamic heating conditions is illustrated in Fig. A.1. The heat of reaction, H, can be expressed mathematically as

$$H_T = \int_{t_o}^{t} \frac{dH}{dt}\, dt \qquad (A.1)$$

However, H_T is calculated in practice by using the following formula

$$H_T = \frac{KxAxRr}{WxS} \qquad (A.2)$$

where

H	--------	Heat of reaction	cal/gm
K	--------	Calibration Constant	1/inch
A	--------	Area under the peak of the curve	$inch^2$
S	--------	Chart recorder speed	inch/sec
Rr	--------	Range (Sensitivity)	mcal/sec
W	--------	Sample Weight	mg

Of these parameters, all of them are instrument parameters which can be set up arbitrarily except the area under the peak of the curve (Fig. A.1).

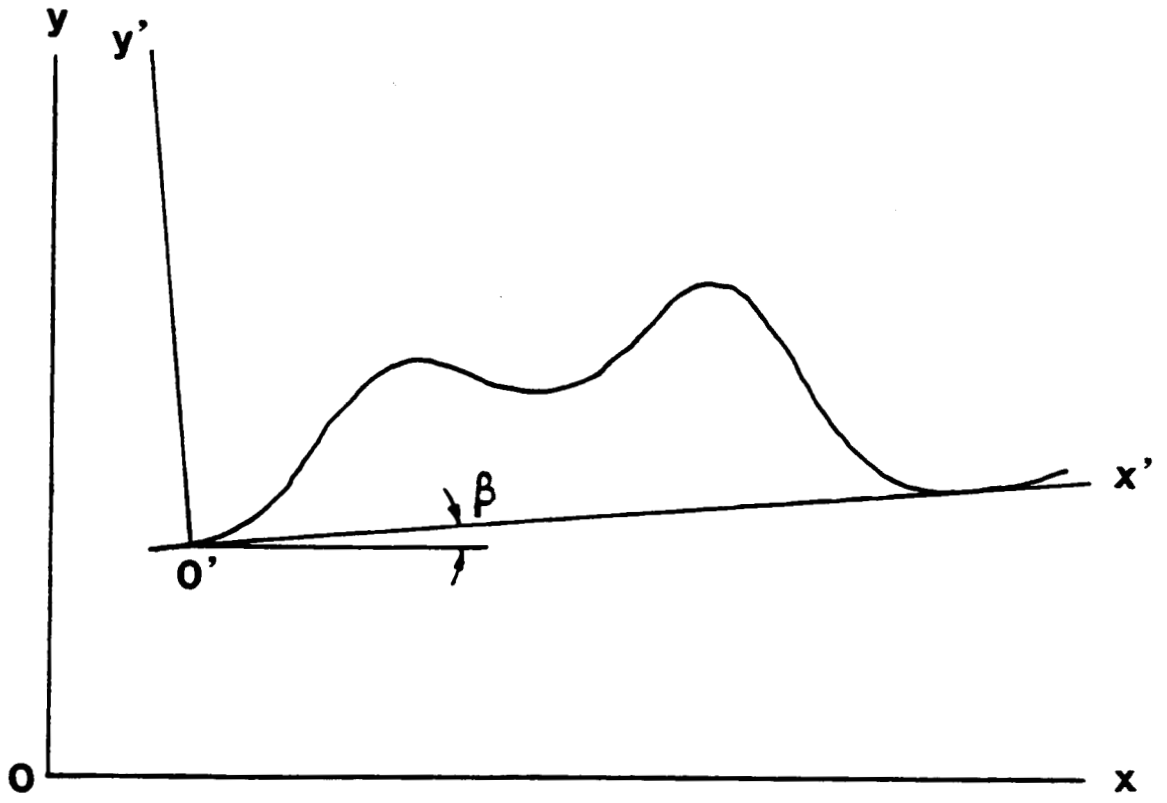

Fig. A.1 Illustration of the DSC thermogram of Hercules 3501-6 in heat of reaction evaluation.

Two numerical techniques, cubic interpolating polynomial approximation and numerical integration were used in the calculation of the area under the peak of the curve obtained from the measurement of heat of reaction by DSC.

For the polynomial interpolation, a set of data is obtained from the curve in the length scale as given below:

x_i (inch) $\quad x_0,\ x_1,\ x_2,\ldots\ldots,x_n$

y_i (inch) $\quad y_0,\ y_1,\ y_2,\ldots\ldots,y_n$

In order to generalize the calculation, the method of interpolation with nonuniformly spaced x values was employed. Similarly, we selected the divided difference method instead of the Lagrangian polynomial method. This permits one to reuse the previous computation if it is desirable to add or subtract a point from the set used to construct the polynomial. Looking at the profile of Fig. A.1, it was presumed that the data could be fitted by a cubic interpolating polynomial. The 3rd-degree polynomial can be written as follows:

$$P_3(x) = a_0 + (x-x_0)a_1 + (x-x_0)(x-x_1)a_2 + (x-x_0)(x-x_1)(x-x_2)a_3 \qquad (A.3)$$

where a_0, a_1, a_2 and a_3 were determined by the divided difference method.

The divided difference is defined as

$$f[x_0, x_1] = \frac{f_1-f_0}{x_1-x_0}$$

$$f[x_o, x_1, x_2] = \frac{f[x_1,x_2] - f[x_o,x_1]}{x_2 - x_o}$$

.

.

.

$$f[x_o,x_1,\ldots,x_i] = \frac{f[x_1,x_2\ldots,x_i] - f[x_o,x_1,\ldots x_{i-1}]}{x_i - x_o}$$

also

$$f(x_o) = f_o$$

It is known that

$$a_o = f_o$$

$$a_1 = f[x_o,x_1]$$

$$a_2 = f[x_o,x_1,x_2]$$

$$a_3 = f[x_o,x_1,x_2,x_3]$$

Thus, Eq. (A.3) can be rewritten as

$$P_3(x) = f_o + (x-x_o)\, f[x_o,x_1] + (x-x_o)\,(x-x_1)\, f[x_o,x_1,x_2] + (x-x_o)\,(x-x_1)\,(x-x_2)\, f[x_o,x_1,x_2,x_3] \qquad (A.4)$$

Equation (A.4) can be applied to every four pairs of grid points. If we had a set of data with (n+1) points just like x_i and y_i, we would get n-1/3 cubic interpolating polynomials.

Let $f(x) = P_3(x) + Rn(x)$

$$E(x) = R_n(x) = (x-x_o)\,(x-x_1)\,(x-x_2)\,(x-x_3)\,\frac{f^{(4)}(\xi)}{(3+1)!}$$

It is well known that when one uses the cubic interpolating polynomial, the magnitude of the error term is

$$E(x) = O(h^4), \qquad \text{if } \lim_{h\to o}(\text{error}) = Kh^4$$

Since the value of h is very small, $E(x) = O(h^4)$ becomes much smaller, then we can approximate

$$f(x) = P_3(x)$$

Thus, the value of f(x) over the entire interval $[x_o, x_n]$ can be computed. Finally, the generalized cubic interpolating polynomial can be expressed as

$$\begin{aligned} f_i(x) &= f_{3i-2} + (x-x_{3i-2})\, f[x_{3i-2}, x_{3i-1}] \\ &\quad + (x-x_{3i-2})(x-x_{3i-1})\, f[x_{3i-2}, x_{3i-1}, x_{3i}] \\ &\quad + (x-x_{3i-2})(x-x_{3i-1})(x-x_{3i})\, f[x_{3i-2}, x_{3i-1}, x_{3i}, x_{3i+1}] \end{aligned} \qquad (A.5)$$

where $i = 1, 2, 3, \ldots, (n-1)/3$

Since every desired value of all points over the entire interval can be obtained by cubic interpolating polynominal mentioned above, the numerical integration would be applied directly upon those points. Before conducting the numerical integration, the coordinate transformation is needed since the baseline of the curve obtained from the experiments does not remain horizontal. Using the following formula

$$\begin{aligned} x_i' &= (x_i - x_o)\cos\beta + (y_i - y_o)\sin\beta \\ y_i' &= -(x_i - x_o)\sin\beta + (y_i - y_o)\cos\beta \end{aligned} \qquad (A.6)$$

where $i = 1, 2, 3, \ldots, n$ $\qquad \beta = \tan^{-1}\dfrac{f(x_n)-f(x_o)}{x_n - x_o}$

a new set of data in prime coordinates can be obtained as

$$x_i': \quad x_o', x_1', x_2', \ldots, x_n'$$

$$y_i': \quad y_o', y_1', y_2', \ldots, y_n'$$

Now, the divided difference and Eq. (A.4) in the prime coordinates can be obtained and a series value of $f(x')$ can be calculated.

In calculating the area under the peak of curve, the Simpson Rule [11], is employed and this is given by

$$A = \int_{x_o}^{x_2} f(x)\,dx = \frac{h}{3}(f_o+4f_1+f_2) + \frac{h^5}{90} f^{(4)}(\xi) \quad x_o < \xi < x_2 \qquad (A.7)$$

where $\frac{h^5}{90} f^{(4)}(\xi) = O(h^5)$ a local error

Equation (A.7) can be applied on every three pairs of grid points for a whole set of data. Thus, for entire interval (x_o, x_n), the total area should be calculated by the following equation

$$A = \frac{h}{3} \sum_{i=1}^{n} (f_{i-1}+4f_i+f_{i+1}) - \frac{x_n - x_o}{180} h^4 f^{(4)}(\xi) \quad x_o < \xi < x_n \qquad (A.8)$$

where $\frac{x_n - x_o}{180} h^4 f^{(4)}(\xi) = O(h^4)$ a global error

Since the value of h selected is very small, $O(h^4)$ becomes much smaller, and one may approximate the area by

$$A = \frac{h}{3} \sum_{i=1}^{n} (f_{i-1}+4f_i+f_{i+1}) \qquad (A.9)$$

A program for calculating the area by employing the above procedure has been coded and listed in Appendix B.

APPENDIX B

COMPUTER CODE FOR APPENDIX A

```
      DIMENSION MATER(25),X(60),Y(60),TABLE(60,60),YFINER(1000)
      DIMENSION XFINER(1000),XPRIM(1000),YPRIM(1000)
C
C... INPUT MATERIAL PROPERTIES ...
      READ(23,10) (MATER(I),I=1,25)
      WRITE(6,20) (MATER(I),I=1,25)
   10 FORMAT(25(A4))
   20 FORMAT(5X,25(A4))
      READ(23,*)WEIGHT,RANGE,HEAT,CHAR,HOLDT,GRTHT,ALPHA,CK,CM,CN
      WRITE(6,30)WEIGHT,RANGE,HEAT,CHAR,HOLDT,GRTHT,ALPHA,CK,CM,CN
   30 FORMAT(/5X,'WEIGHT            =',F6.2,' (MG)',
     *       /5X,'RANGE             =',F6.2,' (MCAL/SEC)',
     *       /5X,'HEAT RATE         =',F6.2,' (K/MIN)',
     *       /5X,'CHART REC.        =',F6.2,' (INCH/SEC)',
     *       /5X,'HOLDING TEMP.     =',F6.2,' (K)',
     *       /5X,'GRAND TOTAL HEAT =',F6.2,' (MCAL)',
     *       /5X,'MAX. DEG. OF CURE =',F7.5,' (100%)',
     *       /5X,'MODEEL LINE SLOPE =',F7.5,
     *       /5X,'EXPONTL,M         =',F7.5,
     *       /5X,'EXPONTL,N         =',F7.5)
C
C... READ DATA AND PRINT ...
      READ(23,*) N,M,XOFF,IBETA,(X(I),Y(I),I=1,N)
      WRITE(6,100) N,M,XOFF,IBETA,(X(I),Y(I),I=1,N)
  100 FORMAT(5X,'THE NUMBER OF INPUT VALUES =       ',I5,
     *      /5X,'THE ORDER OF DIVIDED DIFFERENCED =',I5,
     *      /5X,'X AXIS OFF SET             =',F9.5,' (INCH)',
     *      /5X,'REF. INDEX ROTATION ANGLE =',I5,
     *      //14X,'TIME(INCH)',3X,'HEAT GENERATION(INCH)',
     *      /(10X,F13.6,3X,F13.6))
C
C... UNIT TRANFORMATION ...
      DO 50 I=1,N
      X(I)=(X(I)+XOFF)*CHAR/60.
      Y(I)=Y(I)*RANGE/10.
   50 CONTINUE
      BETA=ATAN(Y(IBETA)-Y(1))/(X(IBETA)-X(1))
      WRITE(6,70) BETA
   70 FORMAT(/5X,'ROTATION ANGLE FOR PRIME COORD.=',E13.5)
C
C... COMPUTE AND PRINT DIVID DIFFERENCES ...
      NAXIS=1
  202 CONTINUE
      NK=N
      CALL DTABLE(X,Y,TABLE,N,M,IFLAG,NK)
      IF(IFLAG.NE.0) GO TO 101
      WRITE(6,200)
      NM1=N-1
      DO 6 I=1,NM1
      L=I
      IF(I.GT.M) L=M
    6 WRITE(6,201)(TABLE(I,J),J=1,L)
C     6  CONTINUE
  200 FORMAT(//5X,'THE DIVIDED DIFFERENCES TABLE ARE :')
  201 FORMAT(10X,3E13.5)
C
C... FINER FUNCTION EVALUATION, BASE ON CUBIC INTERPOLATION POLY.
      IF(NAXIS.EQ.1)XFINER(1)=X(1)
      IF(NAXIS.EQ.1)YFINER(1)=Y(1)
      IF(NAXIS.EQ.2)XPRIM(1)=X(1)
```

```
      IF(NAXIS.EQ.2)YPRIM(1)=Y(1)
      XINC=.05
      JND=1
      NN=(N-1)/3
      XF=X(1)
      DO 400 I=1,NN
      IND=I*3-2
      FX0=Y(IND)
      X0=X(IND)
      X1=X(IND+1)
      X2=X(IND+2)
      X3=X(IND+3)
401   IF(XF+XINC.GT.X3) GO TO 400
      XF=XF+XINC
      JND=JND+1
      IF(NAXIS.EQ.2) GO TO 404
      XFINER(JND)=XF
      YFINER(JND)=FX0+TABLE(IND,1)*(XF-X0)+TABLE(IND+1,2)*(XF-X0)
     *     *(XF-X1)+TABLE(IND+2,3)*(XF-X0)*(XF-X1)*(XF-X2)
      GO TO 401
404   XPRIM(JND)=XF
      YPRIM(JND)=FX0+TABLE(IND,1)*(XF-X0)+TABLE(IND+1,2)*(XF-X0)
     *     *(XF-X1)+TABLE(IND+2,3)*(XF-X0)*(XF-X1)*(XF-X2)
      GO TO 401
400   CONTINUE
      IF(NAXIS.EQ.2) GO TO 503
      WRITE(6,403) JND,(XFINER(I),I=1,JND)
      WRITE(6,402) (YFINER(I),I=1,JND)
403   FORMAT(/5X,'NUMBER OF FINER TIME GRID POINTS =',I5,
     *       //5X,'FINER TIME GRID POINTS (IN INTIAL COORD.)=',
     *       /(5X,5E13.5))
402   FORMAT(//5X,'FINER FUNCTION VALUES (IN INITIAL COORD.)=',
     *       /(5X,5E13.5))
C
C... COORDINATE TRAFORMATION ...
      X1=X(1)
      Y1=Y(1)
      DO 500 I=1,N
      XI=X(I)
      YI=Y(I)
      X(I)=(XI-X1)*COS(BETA)+(YI-Y1)*SIN(BETA)
      Y(I)=-(XI-X1)*SIN(BETA)+(YI-Y1)*COS(BETA)
500   CONTINUE
      NAXIS=2
      GO TO 202
503   WRITE(6,501) JND,(XPRIM(I),I=1,JND)
      WRITE(6,502) (YPRIM(I),I=1,JND)
501   FORMAT(/5X,'NUMBER OF FINER TIME POINTS IN PRIME AXIS =',I5,
     *       /5X,'FINER TIME GRID POINTS (IN NEW COORD.)=',
     *       /(5X,5E13.5))
502   FORMAT(//5X,'FINER FUNCTION VALUES (IN NEW COORD.)=',
     *       /(5X,5E13.5))
C
C... SIMPSON RULE INTEGRATION ...
      ITOT=JND/2
      ITOTAL=ITOT*2
      CALL SIMPTB(ITOTAL,AREA1,YPRIM,XINC)
      AREA=AREA1*60.
      TOTALE=AREA/WEIGHT*10.
      AREA=AREA*1./CHAR*10./RANGE
```

```
      WRITE(6,600) AREA,TOTALE
  600 FORMAT(//5X,'TOTAL AREA (INCH**2. IN NEW COORD.,=',E13.5,
     *        /5X,'HEAT (MCAL)=',E13.5)
C
C... SPECIAL FUNCTION EVALUATION ...
      WRITE(6,700)
      ICOUNT=2
  702 IF(ICOUNT.GE.ITOTAL) GO TO 799
      CALL SIMPTB(ICOUNT,AREA2,YPRIM,XINC)
      AREA2=AREA2*60.
      TOTALP=AREA2/WEIGHT*10.
      RATIO=TOTALP/TOTALE
      FUN1=YPRIM(ICOUNT+1)/WEIGHT
      FUN2=YPRIM(ICOUNT+1)/TOTALE/WEIGHT
      FUN3=ALOG(FUN2)
      FUN4=RATIO
      FUN5=ALOG(FUN4)+(1-ALPHA)/ALPHA*ALOG(1-FUN4)
      FUN6=TOTALE*CK*FUN4**CM*(1-FUN4)**CN
      WRITE(6,701) XPRIM(ICOUNT+1),FUN1,FUN2,FUN3,FUN4,FUN5,FUN6
      ICOUNT=ICOUNT+2
      GO TO 702
  700 FORMAT(//5X,'*** SPECIAL FUNCTION EVALUATION AT SELECTED
     * TIME ***',/
     * /10X,'FUN1= Y"          ',
     * /10X,'FUN2= Y"/H(T)     ',
     * /10X,'FUN3= ALOG(Y"/H(T)) ',
     * /10X,'FUN4= H(I)/H(T)    ',
     * /10X,'FUN5=ALOG(H(I)/H(T))-(1-ALPHA)/ALPHA*ALOG(1-H(I)/H(T))',
     * /10X,'FUN6=H(T)*K*(H(I)/H(T))**M(1-H(I)/(H(T))**N',
     * //2X,'X"(MIN)',3X,'FUN1',7X,'FUN2',8X,'FUN3',7X,'FUN4',
     * 7X,'FUN5',7X,'FUN6',/2X,'-------------------------------------',
     *'------------------------------')
  701 FORMAT(/1X,(2F8.5),5(1X,E11.5))
  799 CONTINUE
      STOP
      END
C
CZZZZZZZZZZZZZZZZZZZZZZZZZZZZZZZZZZZZZZZZZZZZZZZZZZZZZZZZZZZZZZZZZZZZZ
C
      SUBROUTINE DTABLE(X,Y,TABLE,N,M,IFLAG,K)
      DIMENSION X(60),Y(60),TABLE(60,60)
      IF(M.LT.N) GO TO 2
      IFLAG=1
      RETURN
    2 NM1=N-1
      DO 3 I=1,NM1
    3 TABLE(I,1)=(Y(I+1)-Y(I))/(X(I+1)-X(I))
      IF(M.LE.1) GO TO 6
      DO 5 J=2,M
      DO 5 I=J,NM1
      ISUB=I+1-J
    5 TABLE(I,J)=(TABLE(I,J-1)-TABLE(I-1,J-1))/(X(I+1)-X(ISUB))
    6 IFLAG=0
      RETURN
      END
C
CZZZZZZZZZZZZZZZZZZZZZZZZZZZZZZZZZZZZZZZZZZZZZZZZZZZZZZZZZZZZZZZZZZZZZ
C
      SUBROUTINE SIMPTB(N,A,F,DX)
      DIMENSION F(1)
```

```
      A=0.
      M=N/2
      IF(2*M.NE.N) STOP
      DO 10 I=1,M
      K=2*I
10    A=A+F(K-1)+4.*F(K)+F(K+1)
      A=A*DX/3.
      RETURN
      END
```

END

DATE

OCT. 20, 1987